Taylor & Francis
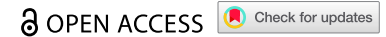Taylor & Francis Group

REPORT

OPEN ACCESS | Check for updates

CC-96673 (BMS-986358), an affinity-tuned anti-CD47 and CD20 bispecific antibody with fully functional fc, selectively targets and depletes non-Hodgkin's lymphoma

Dan Zhu[a], Haralambos Hadjivassiliou[a], Catherine Jennings[a], David Mikolon[a], Massimo Ammirante[b], Sharmistha Acharya[a], Jon Lloyd[a#], Mahan Abbasian[a^], Rama Krishna Narla[b], Joseph R. Piccotti[c*], Katie Stamp[c], Ho Cho[a&], and Kandasamy Hariharan[a]

[a]Department of Discovery Biotherapeutics, Bristol Myers Squibb, San Diego, CA, USA; [b]Oncogenesis Thematic Research Center, Bristol Myers Squibb, San Diego, CA, USA; [c]Department of Nonclinical Development, Bristol Myers Squibb, San Diego, CA, USA

ABSTRACT

Cluster of differentiation 47 (CD47) is a transmembrane protein highly expressed in tumor cells that interacts with signal regulatory protein alpha (SIRPα) and triggers a "don't eat me" signal to the macrophage, inhibiting phagocytosis and enabling tumor escape from immunosurveillance. The CD47-SIRPα axis has become an important target for cancer immunotherapy. To date, the advancement of CD47-targeted modalities is hindered by the ubiquitous expression of the target, often leading to rapid drug elimination and hematologic toxicity including anemia. To overcome those challenges a bispecific approach was taken. CC-96673, a humanized IgG1 bispecific antibody co-targeting CD47 and CD20, is designed to bind CD20 with high affinity and CD47 with optimally lowered affinity. As a result of the detuned CD47 affinity, CC-96673 selectively binds to CD20-expressing cells, blocking the interaction of CD47 with SIRPα. This increased selectivity of CC-96673 over monospecific anti-CD47 approaches allows for the use of wild-type IgG1 Fc, which engages activating crystallizable fragment gamma receptors (FcγRs) to fully potentiate macrophages to engulf and destroy CD20$^+$ cells, while sparing CD47$^+$CD20$^-$ normal cells. The combined targeting of anti-CD20 and anti-CD47 results in enhanced anti-tumor activity compared to anti-CD20 targeting antibodies alone. Furthermore, preclinical studies have demonstrated that CC-96673 exhibits acceptable pharmacokinetic properties with a favorable toxicity profile in non-human primates. Collectively, these findings define CC-96673 as a promising CD47 × CD20 bispecific antibody that selectively destroys CD20$^+$ cancer cells via enhanced phagocytosis and other effector functions.

Introduction

CD47 is an ubiquitously expressed membrane protein that plays a critical role in innate and adaptive immune cell activation.[1] It interacts with SIRPα expressed by macrophages, one of its major binding partners. The CD47-SIRPα axis is an important innate immune checkpoint regulating the homeostatic clearance of aged or damaged cells by macrophages.[2,3] The interaction of CD47 with SIRPα promotes the localization of SIRPα to the phagocytic synapse, activating the src-homology-2 domain containing tyrosine phosphatases (SHP-1 and SHP-2), which ultimately inhibit myosin II accumulation at the phagocytic synapse, preventing engulfment.[4] Interaction of CD47 on cell surfaces with SIRPα on phagocytes thus prevents the phagocytic elimination of healthy cells, serving as a "don't eat me" signal.[5] However, cancer cells have evolved to hijack the CD47-SIRPα axis by upregulating the expression of CD47 to evade macrophage-mediated immune surveillance.[3,6] Overexpression of CD47 was reported in both solid tumors and hematological malignancies.[7–11] Accordingly, blockade of the CD47–SIRPa interaction is considered as a powerful means to activate the phagocytic clearance of tumor cells.[12,13] Therapeutic targeting of the SIRPα–CD47 pathway has been demonstrated to enhance the phagocytic uptake of tumor cells by macrophages *in vitro* and inhibit progression of malignancy in preclinical studies employing various types of tumors.[12,14–21] While many anti-CD47-SIRPα agents are being tested in clinical trials,[22–25] the ubiquitous expression of CD47 limits the selective distribution of antibodies to tumors, leading to the risk of on-target toxicity resulting from phagocytosis of normal cells expressing CD47, including red blood cells (RBCs).[26] Therefore, the development of a molecule that blocks tumor CD47 interaction with SIRPα on macrophages while minimizing its binding to CD47 on normal healthy cells is highly desirable.[27] Recent reports describe next-generation CD47-blocking agents possessing such attributes.[18,28–35] In particular, bispecific antibodies

CONTACT Dan Zhu ✉ dan.zhu@bms.com 🖅 Department of Discovery Biotherapeutics, Bristol Myers Squibb, 10300 Campus Point Drive Suite 100, San Diego, CA 92121
#Current address: Takeda Pharmaceuticals, San Diego, CA, USA.
^Current address: Yitari Bio, San Diego, CA, USA.
*Current address: Schrodinger, San Diego, CA, USA.
&Current address: Samsung Bioepis, Incheon, South Korea.

(BsAb) targeting CD47 and tumor antigens, including NI-1701 for CD47-CD19,[34] IMM0306 for CD47-CD20,[35] and IBI332 for CD47-PD-L1,[35] can selectively block CD47–SIRPα interaction and significantly enhance *in vitro* tumor cell phagocytosis, but with limited effect on RBCs. These findings indicate the promise of dual targeting with the affinity modification approach to balance efficacy and off-target toxicity. Previous preclinical studies have demonstrated that extranodal dissemination of non-Hodgkin lymphoma (NHL) requires CD47, and blocking the CD47–SIRPα interaction may inhibit hematogenous dissemination of primary lymphoma cells and reduce spread to sites such as the central nervous system.[36] Antibodies targeting the CD47–SIRPα interaction have been effective in eliminating tumor cells in both *in vitro* phagocytosis assays and lymphoma xenograft models.[1] Rituximab, a recombinant monoclonal antibody (mAb) against the CD20 antigen that remains the cornerstone of treatment for CD20-positive NHL, has demonstrated synergy with SIRPα-CD47 blockade therapy to enhance the phagocytosis of NHL cells.[36,37] Early clinical data describing magrolimab (an anti-CD47 antibody) in combination with rituximab has shown preliminary activity in relapsed or refractory (R/R) diffuse large B cell lymphoma (DLBCL) and follicular lymphoma (FL).[38] Additionally, preclinical efficacy and safety data suggest that an anti-CD47 BsAb, which simultaneously blocks CD47 and CD19 or CD20, may provide a viable therapeutic option for patients with B cell lymphoma.[29,30,34,39]

Here we report the preclinical characterization of CC-96673, a humanized IgG1 BsAb co-targeting CD47 and CD20. CC-96673 pairs a high-affinity CD20 binding arm with an optimally detuned anti-CD47 arm to drive selective CD47 blockade in $CD20^+$ cells, while minimizing the impact on $CD20^- CD47^+$ normal cells. We demonstrate that CC-96673 potently blocks the CD47–SIRPα interaction and activates macrophage-mediated killing of $CD20^+$ lymphoma cells. With a wild-type IgG1 Fc, CC-96673 also exhibits antibody-dependent cellular cytotoxicity (ADCC) and complement-dependent cytotoxicity (CDC) against CD20-positive tumor cells. CC-96673 does not bind human or cynomolgus monkey RBCs and does not induce hemagglutination/agglutination of human erythrocytes, consistent with its reduced affinity for the human and cynomolgus monkey CD47 protein. CC-96673 demonstrates potent anti-tumor activity in CD20-positive NHL xenograft models. Importantly, CC-96673 displays favorable elimination kinetics and selective depletion of cynomolgus monkey B cells, with minimal drug-related deleterious effects seen on hematologic parameters following multiple administrations to non-human primates. Together, these results warrant the clinical development of CC-96673 as a single agent in B cell lymphoma patients who are refractory and/or resistant to current therapies.

Results

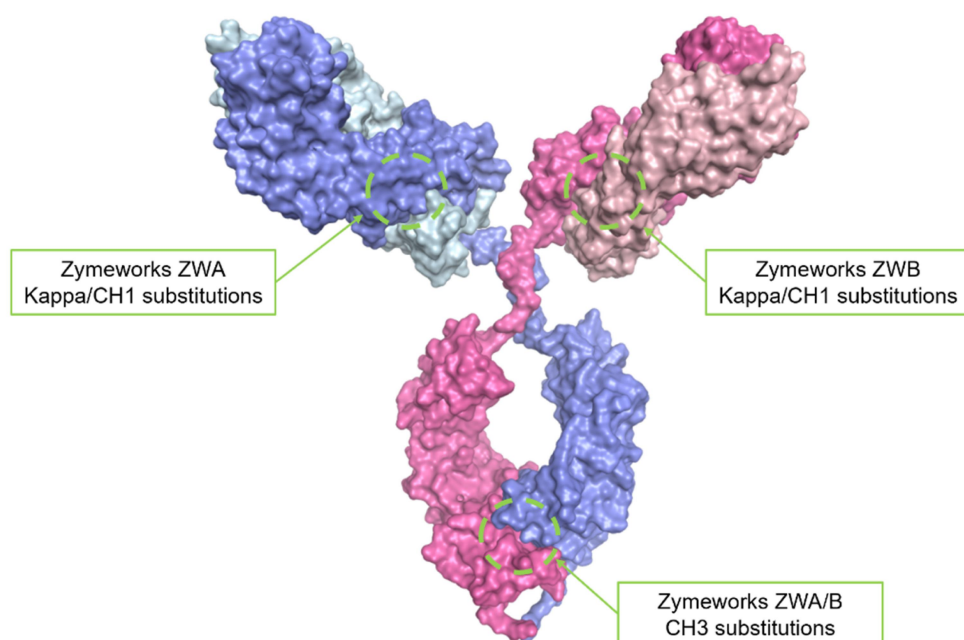### Antibody engineering and characterization of CC-96673

The variable light (VL) and variable heavy (VH) sequences of an optimally detuned variant of Celgene's CD47 antibody CC-90002,[21] and the VL and VH sequences of rituximab were engineered into kappa light and IgG1 heavy-chain constructs containing Zymeworks Azymetric substitutions[40] to construct the humanized BsAb, CC-96673 (Figure 1a). Specifically, a next-generation CC-90002 VH/VL pair (408/437) was used as a starting point to identify an anti-CD47 variant with the optimally detuned affinity. Taking advantage of an internal crystal structure of the anti-CD47 408/437 antigen-binding fragment (Fab) bound to the extracellular domain (ECD) of human CD47, we utilized the Molecular Operating Environment (MOE) software[41] to carry out *in silico* mutagenesis on the anti-CD47 paratope residues. The predicted differences in affinities and stabilities between the variants and the parental anti-CD47 Fab sequence were calculated in MOE, and variants were screened *in silico* for the introduction of immunogenic motifs using Epivax MHC II peptide prediction software[42] (Figure 1b). A total of 143 variants with a range of predicted affinities, acceptable stabilities, and lacking immunogenic liabilities were selected to construct a library of detuned anti-CD47 Fab variants. These variable domains were engineered as IgG1 BsAbs and initially paired with the anti-epidermal growth factor receptor (EGFR) arm from cetuximab to enable screening to find the optimally detuned anti-CD47 Fabs.

Non-target cell binding was assessed by measuring the binding of the detuned CD47 BsAb to $CD47^+EGFR^-$ Raji cells. Target cell binding was assessed by measuring the ability of the detuned CD47 × EGFR BsAb to block SIRPα binding to $CD47^+EGFR^+$ FaDu target cells. From these experiments, we identified a group of optimally detuned CD47 BsAbs that showed minimal binding to the non-target $CD47^+EGFR^-$ Raji cells relative to the non-detuned CD47 × EGFR parental antibody and yet were still able to block 75% to 90% of SIRPα binding to the target $CD47^+EGFR^+$ FaDu target cells (Figure 1c). The VL and VH sequences of the most optimally detuned anti-CD47 E59Y/S102E variant and the anti-CD20 VL/VH sequences from rituximab were then molecularly cloned into kappa light chain (LC) and IgG1 heavy chain (HC) vectors to form the lead candidate CC-96673 (Figure 1a). Kappa LC and IgG1 HC vectors contain Zymeworks substitutions in the constant light and heavy regions (Figure 1a) to enable proper heterodimeric pairing of the LCs and the Fc.

CC-96673 binding to captured human and cynomolgus monkey CD47 was assessed by measuring the kinetic on- and off-rate under affinity conditions. CC-96673 demonstrated calculated K_D values of 2.32 μM for human CD47 and 23.0 μM for cynomolgus monkey CD47 (Table S1). CC-96673 displayed high-affinity binding to human CD20, with calculated K_D values of 13.8 nM (Table S2), comparable to rituximab CD20 binding affinity with calculated K_D values of 5.6 nM. Structural analysis demonstrated that CC-96673 binds to the region of CD47 previously identified to be recognized by SIRPα (Figure 1b). First, the levels of CD47 and CD20 expression on the cell surface of various lymphoma cell lines were evaluated and quantified as antibody-binding capacity (ABC) value (Figure 1d). Then, the ability of CC-96673 to block the interaction of recombinant human SIRPα with cell surface CD47 on the lymphoma cells was analyzed by preincubation with various concentrations of CC-96637 followed by flow cytometry. Blocking IC_{50} values and maximum percent

a.

b.

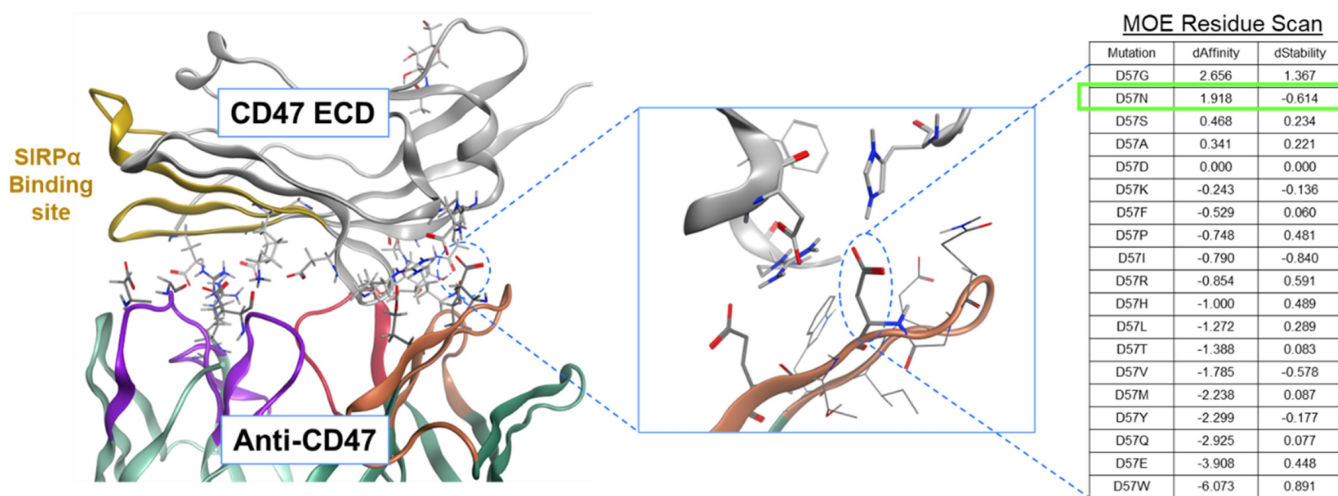| MOE Residue Scan		
Mutation	dAffinity	dStability
D57G	2.656	1.367
D57N	1.918	-0.614
D57S	0.468	0.234
D57A	0.341	0.221
D57D	0.000	0.000
D57K	-0.243	-0.136
D57F	-0.529	0.060
D57P	-0.748	0.481
D57I	-0.790	-0.840
D57R	-0.854	0.591
D57H	-1.000	0.489
D57L	-1.272	0.289
D57T	-1.388	0.083
D57V	-1.785	-0.578
D57M	-2.238	0.087
D57Y	-2.299	-0.177
D57Q	-2.925	0.077
D57E	-3.908	0.448
D57W	-6.073	0.891

Figure 1a. CC-96673, a CD47×CD20 bispecific antibody with an optimally detuned CD47 arm, blocks recombinant SIRPα binding to cell surface CD47. (a) Design of CC-96673 CD47×CD20 zymeworks IgG1. (b) anti-CD47 structure guided detuning strategy.

inhibition by CC-96673 were calculated in five CD20^{+}/CD47^{+} lymphoma cell lines expressing various level of CD47 and CD20 (Figure 1d). In these cell lines with CD20/CD47 protein ratio at or above 0.5, CC-96673 demonstrated blocking of SIRPα binding to CD47 with calculated IC_{50} values ranging from 0.75 to 5.62 nM (Figure 1d and Figure S1a). At a top concentration of 66.6 nM, 91.0% to 96.8% (94.2% ± 0.6) of recombinant SIRPα was inhibited from binding to human CD47 by CC-96673 (Figure 1d), comparable to the positive control, a monospecific and bivalent anti-CD47 IgG1 with non-attenuated affinity (TPP-23). Conversely, rituximab and the anti-CD20 × hen egg lysozyme (HEL) BsAb antibody control were unable to compete with human SIRPα-Fc binding

to the same cell lines (Figure S1b), which suggests that the detuned anti-CD47 arm of CC-96673 is critical for blocking the SIRPα-CD47 pathway. In a DLBCL cell line with a CD20/CD47 ratio of 0.2, WSU-FSCCL, CC-96673 demonstrated only moderate blocking of recombinant SIRPα binding to cell surface CD47 (29.8 ± 3.9%), confirming its dependence on CD20 for avidity-driven binding to CD47 (Figure S1a). On cell surfaces displaying significantly more CD47 antigen than CD20 antigen, CC-96673 may bind only the portion of CD47 proteins located within proximity to CD20, leaving some CD47 molecules available for SIRPα interaction.

To ensure sufficient detuning of the anti-CD47 arm, CC-96673 binding to human RBCs was initially assessed by flow

c.

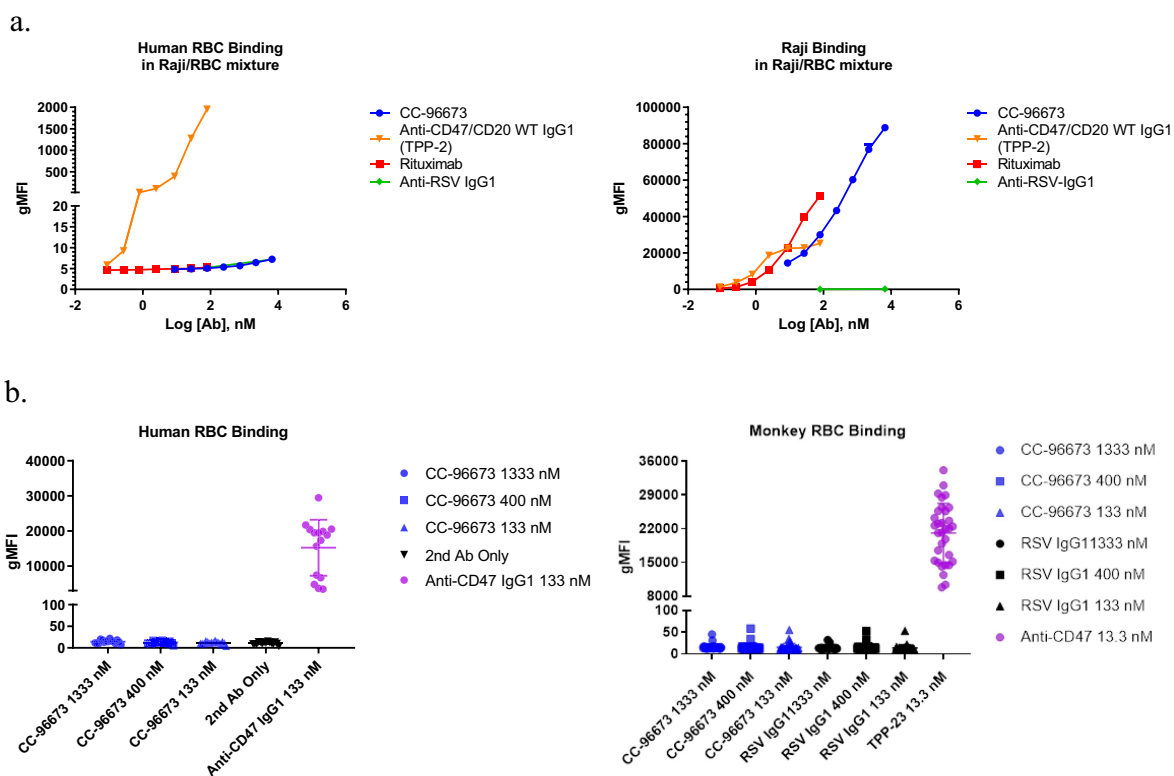Detuned anti-CD47 variants ordered by affinity to non-target cells
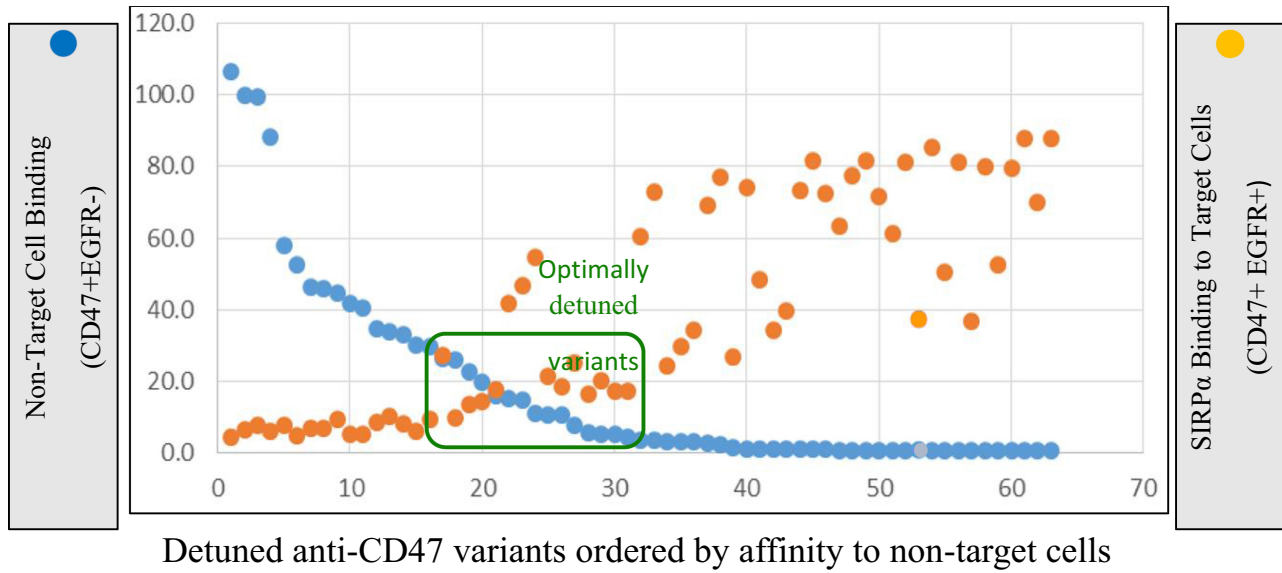
d.
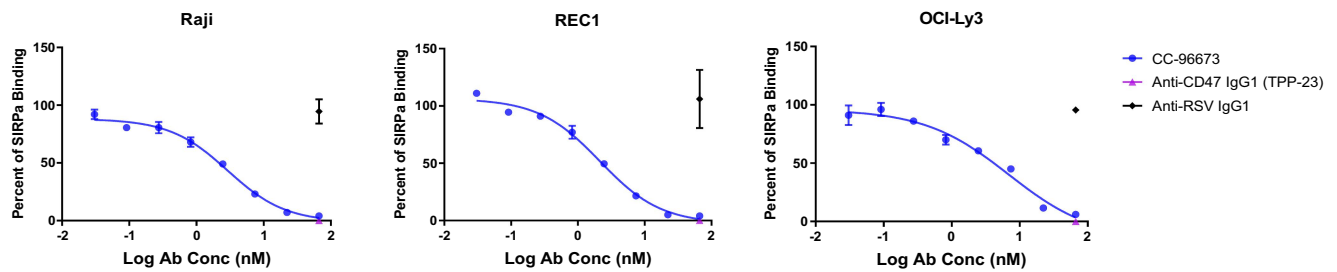
Cell Line	CD20 ABC Mean ± SD	CD47 ABC Mean ± SD	IC$_{50}$ (nM) Mean ± SD	Maximal Inhibition (%) Mean ± SD
WSU-DLCL2	1236740 ± 249673	166014 ± 71672	0.75 ± 0.19	91.0 ± 1.4
Raji	520617 ± 2799	220961 ± 9947	2.91 ± 0.02	95.5 ± 0.7
REC1	569932 ± 84706	607265 ± 217576	1.98 ± 0.21	96.8 ± 0.4
RIVA	387820 ± 442	473265 ± 19121	2.97 ± 0.41	93.5 ± 0.7
OCI-Ly3	131000 ± 32527	239500 ± 10607	5.62 ± 1.80	94.0 ± 0.0
WSU-FSCCL	86028 ± 9342	403734 ± 89102	> 66.6	29.8 ± 3.9

Figure 1b. (c) Screening strategy for an optimally detuned anti-CD47 fab. A library of detuned CD47×EGFR bispecifics were screened for minimal binding to non-target CD47$^+$EGFR$^-$ Raji cells and maximum inhibition of SIRPα binding to CD47$^+$EGFR$^+$ FaDu cells. (d) Top: Representative curves of recombinant SIRPα binding to CD47 on the surface of each lymphoma cell line evaluated in the presence of CC-96673. Bottom: a summary of IC50 values and maximum percent inhibition of recombinant SIRPα binding to cell surface CD47 by CC-96673. The surface expression of CD47 and CD20 on NHL cell lines was determined using the QSC anti-human IgG kit and antibody-binding capacity (ABC) values were calculated automatically using the QuickCal template. Each symbol represents mean percent of control of SIRPα binding with error bars depicting standard deviation (SD) of two independent experiments.

cytometry in mixtures of Raji tumor cells with a 10-fold excess of human RBCs. CC-96673 displayed dose-dependent binding to CD47$^+$CD20$^+$ Raji cells, but no binding to CD47$^+$CD20$^-$ RBCs (Figure 2a). In this model, the CC-96673 binding profile was comparable to that of rituximab, indicating that CD20 expression is necessary for CC-96673 binding. Conversely, TPP-2, a CD47 × CD20 BsAb with a non-attenuated anti-CD47 arm, showed dose-dependent binding to both Raji

cells and human RBCs, while the negative control anti-respiratory syncytial virus (RSV) IgG1 antibody did not bind either Raji cells or human RBCs. Furthermore, the binding of CC-96673 to freshly isolated human and cynomolgus monkey RBCs was extensively evaluated across a range of concentrations, up to 1333.3 nM. At all tested concentrations, CC-96673 did not bind RBCs purified from whole blood samples from healthy human ($n = 15$) and monkey donors ($n = 32$), similar

a.

Human RBC Binding in Raji/RBC mixture

Raji Binding in Raji/RBC mixture

Legend (both plots):
- CC-96673
- Anti-CD47/CD20 WT IgG1 (TPP-2)
- Rituximab
- Anti-RSV IgG1

X-axis: Log [Ab], nM; Y-axis: gMFI

b.

Human RBC Binding

Legend:
- CC-96673 1333 nM
- CC-96673 400 nM
- CC-96673 133 nM
- 2nd Ab Only
- Anti-CD47 IgG1 133 nM

Monkey RBC Binding

Legend:
- CC-96673 1333 nM
- CC-96673 400 nM
- CC-96673 133 nM
- RSV IgG11333 nM
- RSV IgG1 400 nM
- RSV IgG1 133 nM
- Anti-CD47 13.3 nM

X-axis categories (monkey): CC-96673 1333 nM, CC-96673 400 nM, CC-96673 133 nM, RSV IgG11333 nM, RSV IgG1 400 nM, RSV IgG1 133 nM, TPP-23 13.3 nM

c. CC-96673 Primarily Binds B Cells in Human Whole Blood

Human Whole Blood Subsets	CC-96673 Binding Mean gMFI ± SD	RSV IgG1 Binding Mean gMFI ± SD
B cells	2329.5 ± 1034.5	229.5 ± 14.8
NK cells	712.0 ± 213.5	153.0 ± 87.8
T cells	194.5 ± 68.6	128.4 ± 66.0
Monocytes	561.5 ± 61.5	378.5 ± 55.9
RBCs	27.4 ± 1.5	24.8 ± 1.3
Platelets	164.0 ± 29.7	99.7 ± 35.9

d.

B cell depletion: Emax

*Y-axis: % depletion at top dose; X-axis categories: CC-96673, Rituximab, anti-RSV IgG1; ns; ****

B cell depletion: Potency

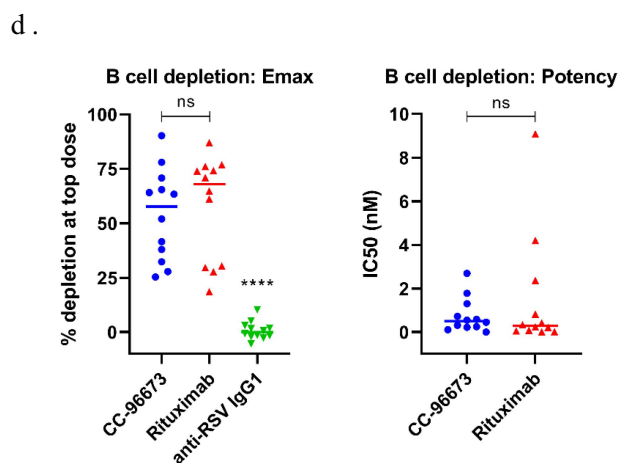*Y-axis: IC50 (nM); X-axis categories: CC-96673, Rituximab; ns*

Figure 2. CC-96673 selectively binds to CD47$^+$CD20$^+$ cells and depletes autologous B cells in human whole blood. (a) CC-96673 binds CD47$^+$CD20$^+$ cells in the presence of excess CD47-only expressing RBCs. Purified human RBCs and Raji cells were combined at a ratio of 10:1 prior to incubation with test antibodies and secondary

to negative control RSV IgG1, while anti-CD47 IgG1 (TPP-23) binds to both human and cyno RBCs (Figure 2b).

The aggregation of RBCs represents a major limitation to the therapeutic targeting of CD47,[23,38] owing to the relatively high expression levels on erythrocytes.[43,44] CC-96673 was analyzed for hemagglutination capacity using RBCs from healthy human donors ($n = 4$). The anti-CD47 antibody BRIC126 was used as a positive control[43] and elicited hemagglutination, while CC-96673 and the negative control anti-RSV IgG1 did not (Figure S2). Furthermore, whole blood samples from healthy adult donors ($n = 5$) spiked with increasing concentrations of CC-96673 (from 2 nM to 2000 nM) did not show agglutination of RBCs measured under normal (saline) or low ionic buffer (to enhance agglutination) conditions (data not shown). Together, these data support the idea that the CD47 binding affinity of CC-96673 is optimally attenuated, eliminating its binding to CD47$^+$CD20$^-$ cells. The lack of binding to RBCs is an advantage and differentiates CC-96673 from other anti-CD47 antibodies.

To further determine the cellular specificity of CC-96673, an assessment was made of CC-96673 binding to primary human and monkey immune cell subsets in whole blood and peripheral blood mononuclear cells (PBMCs) by multi-parameter flow cytometry. In purified human immune subsets of PBMCs ($n = 2$), CC-96673 at 200 nM bound primarily to B cells (Table S3). This selective binding to B cells was confirmed in human whole blood from healthy donors ($n = 2$) (Figure 2c). This B cell selectivity is expected as CC-96673 binds to CD20 with high affinity and avidity rendered by the dual interaction with both CD20 and CD47 targets. We then evaluated the potency of CC-96673 to deplete human B cells by employing an *ex vivo* B cell depletion assay. By using whole blood and thus autologous target and effector cells, we aimed to better reflect the interplay of multiple cell types found *in vivo*. The potency of an anti-CD20 antibody (rituximab) or anti-CD19 antibody (MOR208) was compared to CC-96673 in B cell depletion assays using heparinized normal human blood samples ($n = 12$). Whole blood was incubated with CC-96673 or control antibodies for 24 h followed by RBC lysis and flow cytometry. B and T cell populations were evaluated by gating on CD45$^+$ lymphocytes and determining the CD3$^+$ T cell and CD19$^+$ or CD79$^+$ B cell populations therein. CC-96673 induced dose-dependent depletion of CD19$^+$ B cells, with a maximum depletion of 55.06 ± 21.89%, not significantly different from rituximab activity ($p = .6515$) (Figure 2d, Figure S3a). The potency of CC-96673 in depleting B cells in human whole blood was also comparable to rituximab, with an average IC$_{50}$ of 0.75 ± 0.8 nM and 1.49 ± 2.7 nM, respectively ($p = .276$). Using CD79b as pan B cell marker, the B cell depletion activity of CC-96673 was then compared to that of the CD19

mAb, MOR208 (Figure S3b). CC-96673 had a significantly greater maximal effect than MOR208, with an average B cell depletion of 61.24 ± 14.97% vs 24.81 ± 27.32%, respectively, at the top dose tested in 12 donors ($p < .0001$).

B cell depletion was then evaluated relative to the matching donor FcγR genotypes and CD20 or CD19 expression, to assess whether the activity of CC-96673 could be associated with FcγR affinity or target abundance in B cells. PBMCs isolated from the donor whole blood samples were used to detect functionally relevant polymorphisms in FCGR2A (rs1801274) and FCGR3A (rs396991) by TaqMan-based qPCR. Allelic discrimination plots showed that 4/12 donors harbored the single nucleotide polymorphism (SNP) encoding the high-affinity FCGR2A (131 H/H); 5/12 donors had the low-affinity FCGR2A (131 R/R) (Figure S3c). The Donor 12 genotype for this SNP could not be determined. The high-affinity version of FCGR3A (158 V/V) was found in only one donor; 7/12 donors were homozygous A/A for this allele, predicting the low-affinity FCGR3A (158F/F) (Figure S3c). No significant relationship was uncovered between donor FCGR2A or FCGR3A SNP status and the B cell depletion activity of the tested antibodies. The surface expression of CD47, CD20, and CD19 was also quantified on B cells in these PBMC samples using fluorescently labeled antibodies to stain both cells and beads coated with Fc-specific capture antibody (data not shown). CD20 levels were relatively uniform across the 12 donors and significantly higher than CD19 density (15983.93 ± 534.15 and 856.87 ± 34.20, respectively; $p < .0001$). Nevertheless, correlation analyses indicated that the potency of CC-96673, rituximab, or MOR208 to deplete B cells was not significantly linked to CD20 or CD19 antigen density. Overall, the B cell depletion capacity of CC-96673 is consistent with its binding profile in human whole blood and could be used as a pharmacodynamic marker in clinical trials.

CC-96673 enhances antibody-dependent phagocytosis of CD20$^+$CD47$^+$ tumor cells

With a wild-type IgG1 Fc, CC-96673 not only targets CD47 to block CD47–SIRPα interactions but also engages activating FcγR family members as assessed by both Biacore-based protein binding (Table S4) and FRET-based cellular binding assays (Table S5). Accordingly, studies were conducted to demonstrate the effect of CC-96673 on the phagocytosis of CD47$^+$CD20$^+$ cancer cell lines *in vitro*. CC-96673 enabled antibody-mediated phagocytosis of a panel of lymphoma cell lines expressing various levels of CD47 and CD20 (Table S6). CC-96673 treatment demonstrated concentration-dependent increases in the percentage of phagocytic macrophages, with the following maximum percent ranges: Raji, 53% to 70% ($n = 3$ macrophage

antibody staining. (b) CC-96673 does not bind to human or cynomolgus monkey RBCs. Purified RBCs were incubated with the indicated concentrations of test antibodies prior to secondary antibody staining. (c) CC-96673 binds primarily to B cells in human whole blood. Whole blood was stained with a fluorochrome-conjugated antibody mix recognizing immune cell subsets (anti-human CD14, CD19, CD56, and CD3) and containing either AF647-labeled CC-96673 or the non-targeting anti-RSV IgG1. Binding to RBCs and platelets was done separately using anti-human GYPA and CD41a, respectively. All cell binding was assessed by flow cytometry and gMFI ± SD is reported. (d) CC-96673 depletes autologous B cells in human whole blood. Whole blood samples were incubated with CC-96673, rituximab or anti-RSV IgG1 for 24 hours, prior to staining and RBC lysis. The percent CD19$^+$ B cell death was determined by flow cytometry. Emax represents percent depletion at the top antibody concentration and IC50 was calculated from each dose response curve. Graphs show the median of individual values from 12 donors. Significant differences assessed by one-way ANOVA using uncorrected Fisher's LSD. ****$p < .0001$, ns = no significance.

donors); OCI-Ly3, 49% to 86% (*n* = 5 macrophage donors); REC-1, 28% to 75% (*n* = 2 macrophage donors); RIVA, 41% to 60% (*n* = 2 macrophage donors) (representative curves shown in Figure 3a and Figure S4a). Area under the curve (AUC) for each dose-response curve of CC-96673 was also calculated and compared to the AUC of the rituximab dose–response curve (Figure 3a). Treatment with CC-96673 triggered significantly more efficient phagocytosis of Raji and OCI-Ly3 than rituximab, with AUC p-values of 0.045 and 0.0009, respectively. Of note, both CC-96673 and another detuned CD47 × CD20 variant (TPP-1362) increased phagocytosis relative to treatment with HEL × anti-CD20 control, while the detuned anti-CD47 arm × HEL controls induced minimal phagocytosis as expected (Figure S4b). These data suggest that inhibition of the CD47-SIRPα "don't eat me" signal via avidity driven binding to CD47 antigen is necessary for the enhanced antibody-dependent cellular phagocytosis (ADCP) activity of CC-96673.

Furthermore, CC-96673 as a single agent was compared to the combination of rituximab and an anti-CD47 IgG4 with serine 228 to proline and leucine 235 to glutamic acid mutations (IgG4PE). In this study, OCI-Ly3 target cells were opsonized with CC-96673, rituximab, or a combination of rituximab and anti-CD47 IgG4PE. Consistently, CC-96673 treatment demonstrated concentration-dependent increases in percent phagocytic macrophages (four donors with repeat tests for three donors, n = 7) (Figure 3b). Dose–response AUC values for CC-96673, rituximab, anti-CD47 IgG4PE, or the

combination of rituximab and anti-CD47 IgG4PE were calculated. CC-96673 single-agent activity was significantly higher than rituximab or anti-CD47 IgG4PE in inducing macrophage-mediated phagocytosis of OCI-Ly3, with mean AUC *p* values of 0.0087 or 0.0425, respectively (Figure 3b). Notably, the mean AUC value of CC-96673 as a single agent to induce phagocytosis of OCI-Ly3 cells was comparable to the phagocytic activity of rituximab and anti-CD47 IgG4PE in combination (Figure 3b).

CC-96673 can induce antibody-dependent cellular cytotoxicity and complement-dependent cytotoxicity

To further investigate CC-96673's ability to engage FcγRs, the extent of ADCC against cells expressing CD47 and CD20 was measured. Induction of CC-96673 mediated ADCC targeting four human lymphoma cell lines (Raji, OCI-Ly3, WSU-FSCCL, and SC-1) was tested *in vitro* by coculture assays using human natural killer (NK) cells from healthy donors. CC-96673 demonstrated potent, concentration-dependent ADCC against the four NHL cell lines with similar levels of CD47 but a range of CD20 expression (Figure 4a, Table S6). Dose–response AUCs for each curve of CC-96673 was compared to rituximab, showing that the capacity of CC-96673 to induce ADCC against CD47⁺CD20⁺ lymphoma cells was significantly greater than that of rituximab (*p* = 0.0181). It has been well documented that a monovalent BsAb (such as CC-
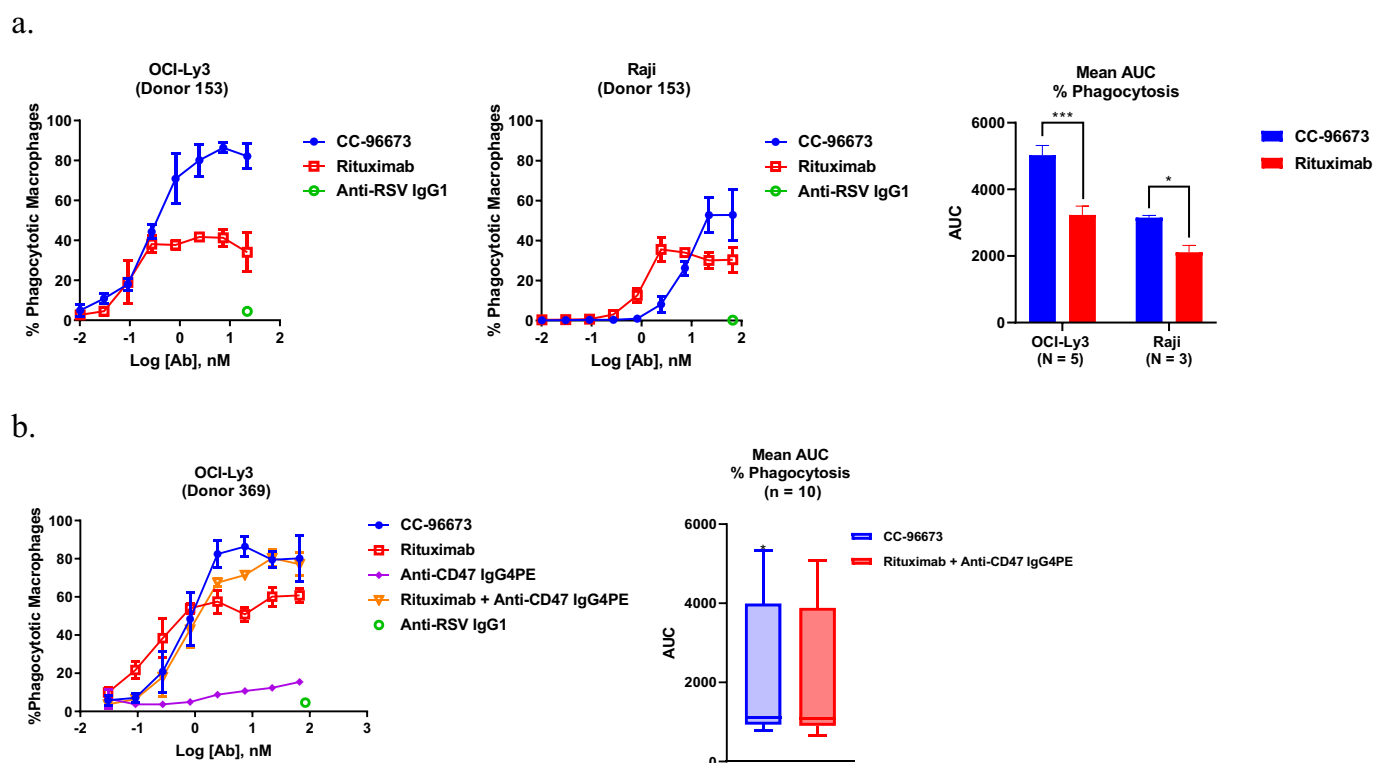

Figure 3. CC-96673 promotes phagocytosis of CD47⁺CD20⁺ lymphoma cells. (a) CC-96673 induces significantly more efficient phagocytosis than rituximab. Antibody-opsonized human macrophages and NHL tumor cells were cocultured for 3 hours prior to imaging. Graphs show representative dose response curves for CC-96673 induced phagocytosis of NHL cells (left) with corresponding AUC data for all macrophage donors (right). (b) CC-96673-induced phagocytic activity is comparable to that of rituximab combined with anti-CD47 IgG4PE. CC - 96,673, rituximab, anti-CD47 IgG4PE, or equal parts rituximab and anti-CD47 IgG4PE were added to cocultures of macrophages and tumor cells. Representative dose response curves for CC-96673 induced phagocytosis of NHL cells (left) with corresponding combined AUC data (right). Dose response values represent the mean of triplicate wells ± SD. AUC values represent the mean of multiple donors ± SEM. N = number of individual macrophage donors tested per cell line. Significant differences assessed by paired t test. ***p < .0005, **p < .005, *p < .05.
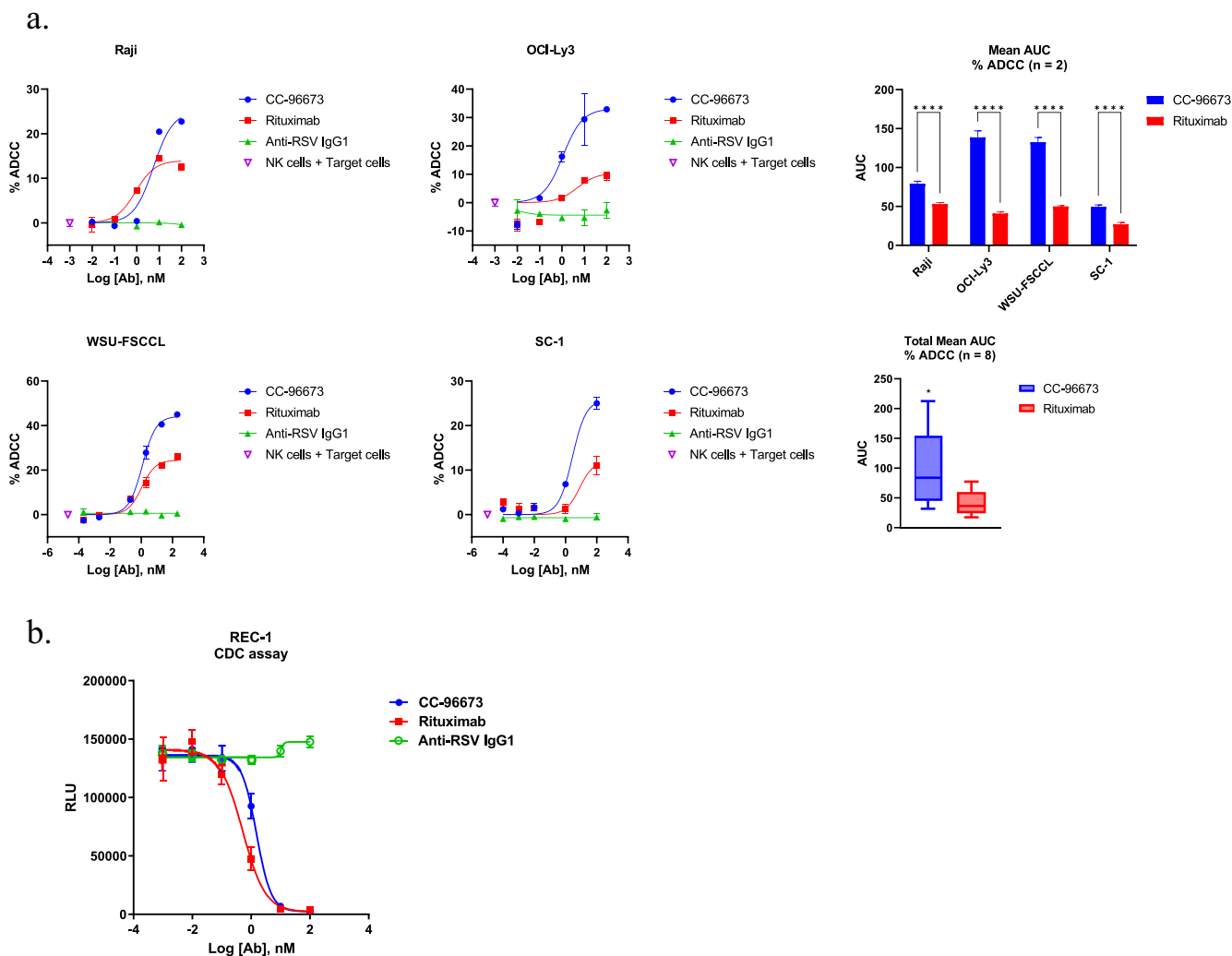
a.

b.

Figure 4. CC-96673 induced ADCC and CDC against CD47+CD20+ lymphoma cells. (a) Antibody-opsonized NHL tumor cells were cocultured with human NK cells for 4 hours prior to flow cytometry to assess tumor cell lysis. Representative dose response curves for CC-96673- induced ADCC (left) with corresponding mean AUC data ± SEM for four NHL cell lines, two NK cell donors each (right). Significance assessed by two-way ANOVA with Sidak's multiple comparison test (****$p < .0001$) or paired t test (*$p < .05$). (b) Antibody-opsonized REC-1 cells were incubated with rabbit serum for 2 hours prior to measuring cell viability by plate reader. Graph shows representative dose response curve of CC-96673-induced CDC activity. RLU = relative light units. All dose response values represent the mean of triplicate wells ± SD.

96673) interacts monovalently with the target antigen and thus occupies one antigen site so that each site is represented by a single Fc. It is therefore feasible that the monovalent binding of CC-96673 will result in increased tumor cell opsonization, compared to a bivalent monospecific antibody such as rituximab, which occupies two antigen sites but presents a single Fc.

To test whether dual engagement of CD20 and CD47 is required for CC-96673's functional response, we assessed its ADCC activity in parallel with monovalent monospecific control molecules constructed by pairing the anti-CD20 or anti-CD47 arm of CC-96673 with an anti-HEL control arm. In NK cell cocultures with four separate CD47+CD20+ lymphoma cell lines, CC-96673 displayed significantly more potent ADCC activity than the anti-CD20 × HEL control molecule (Figure S5). Consistently, CC-96673 showed significantly higher ADCC activity than the monovalent monospecific anti-CD47 × HEL control molecule in two CD47+CD20+ lymphoma cell lines, SC1 and WSU-FSCCL (data not shown). This suggests that the efficacy of CC-96673-induced ADCC

is driven by both Fab arms and that this increased avidity, in addition to the potential for enhanced opsonization, is required for an efficient Fc-mediated response. Furthermore, the Fc domain of CC-96673 showed much higher affinity for FcγR2A, FcγR2B, and FcγR3A, in comparison to the isotype control (Table S4). In line with the SPR data, CC-96673 demonstrated significantly higher binding to cells overexpressing FcγR2A, FcγR2B, or FcγR3A relative to rituximab or the isotype control (Table S5). Taken together, these data propose that the increased ADCC activity of CC-96673 (Figure 4) is mainly driven by its enhanced interaction with FcγR3A on NK cells, in concert with its high-avidity binding to and likely increased opsonization of target cells.

The ability of CC-96673 to induce CDC was also assessed using the NHL cell line, REC-1. CC-96673 demonstrated concentration-dependent lysis of REC-1 target cells in the presence of rabbit complement serum, with an EC_{50} value of 1.37 ± 0.22 nM, comparable to the potency of rituximab (EC_{50} = 0.91 ± 0.55 nM) (Figure 4b).

CC-96673 confers anti-tumor activity in vivo

We then extended our studies to evaluate the antitumor activity of CC-96673 in human lymphoma cell line-derived xenograft models. Here, WSU-DLCL2 DLBCL cells were implanted subcutaneously into non-obese diabetic-severe combined immune deficient (NOD-SCID) mice and allowed to establish a tumor of approximately 250 mm^3 prior to initiation of therapy. Significant dose-dependent antitumor activity was observed with CC-96673 treatment in this WSU-DLCL2 x enograft model with 66% and 86% tumor volume reduction at 10 and 30 mg/kg dosed weekly (QW) (Figure 5a). In this tumor model, CC-96673 exhibited similar antitumor activity to rituximab (69% and 79% tumor volume reductions at 10 and 30 mg/kg QW) (Figure 5a). In the doses tested, no significant loss of body weight or other clinical observations were noted in animals treated with CC-96673. An additional study was conducted to determine the antitumor activity of CC-96673 in a Raji Burkitt lymphoma-derived xenograft model, with QW dosing at 10 and 30 mg/kg in NOD-SCID mice inoculated with 2×10^6 Raji tumor cells into the right flank. Dosing started on Day 11 when the tumor size was approximately 275 mm^3. Significant, but dose-independent, tumor inhibition was achieved with CC-96673 with a 52% tumor volume reduction at 10 and 30 mg/kg QW ($p < .0001$) (Figure 5b). Tumor volume reductions of 33% and 38% were observed with rituximab at 10 and 30 mg/kg QW, respectively (Figure 5). The antitumor activity of CC-96673 at 30 mg/kg QW was significantly greater than that of rituximab at a corresponding dose level ($p < .01$). No significant body weight loss was observed in the groups dosed with an anti-RSV IgG1 antibody, CC-96673, or rituximab. Together, these data corroborate our *in vitro* findings that co-targeting CD47 and CD20 improves tumoricidal activity, translating into improved tumor control *in vivo*.

CC-96673 displays an acceptable pharmacokinetics and favorable safety profile in non-human primates

Next, we evaluated the pharmacokinetic and safety profile of CC-96673 in cynomolgus monkeys after single or repeat dosing. In a single dose pharmacokinetics (PK) study, systemic exposure was observed in all monkeys treated with a single 20 mg/kg intravenous (IV) slow bolus dose of CC-96673 (Table 1). Mean clearance (CL) was 0.29 mL/h/kg and the volume of distribution (Vd) was approximately equal to the plasma volume. The mean elimination half-life (t½) was 2.8 days. Anti-drug antibody (ADA) formation was observed in all three female monkeys and was considered to affect PK. Two repeat-dose toxicology studies were conducted on male and female cynomolgus monkeys to assess toxicokinetic (TK) parameters and pharmacodynamic activity and to determine the potential toxicity of CC-96673. First, an exploratory toxicity study was performed with either weekly (QW) (20 or 100 mg/kg) or twice a week (BIW) (10 mg/kg) dosing for 2 weeks with a 2-week off-dose period. CC-96673 exhibited linear PK with approximately dose-proportional or greater than dose-proportional increases in exposure (Cmax and AUC$_{LST}$) from 20 to 100 mg/kg (Table 1). After the first dose, CL was

similar across the 20 and 100 mg/kg dose range, suggesting target saturation. Vd was slightly higher than the plasma volume and the mean t½ ranged from 2 to 4.5 days (Table 1). Despite the generation and presence of ADA, exposure to circulating free CC-96673 was achieved and maintained throughout the dosing phase at all dose levels, albeit lower in ADA-positive animals (Table S7), enabling appropriate evaluation of potential toxicities. Administration of CC-96673 to cynomolgus monkeys, either BIW or QW, was well-tolerated up to 100 mg/kg QW, the highest dose tested. Decreases in B cells in the peripheral blood and in multiple lymphoid tissues (spleen, lymph node, Peyer's patches) were seen at 10 mg/kg BIW and ≥20 mg/kg QW, demonstrating robust pharmacodynamic activity (Figure 6a–d). In addition to the effects on B cells, CC-96673 also decreased T cells and NK cells at all dose levels, and decreased neutrophils at ≥20 mg/kg QW. After the 14-day non-dosing period, there was evidence of B cell recovery in peripheral blood and in lymphoid tissues, and rising NK cell counts with decreasing exposure, indicating recovery as expected.

We further investigated the safety of CC-96673 in a pivotal toxicity study via slow bolus IV injection into male and female cynomolgus monkeys (3/sex/group) QW at dosage levels of 0, 20, 60, or 100 mg/kg/dose for a period of 4 weeks (5 doses). All animals survived to their scheduled necropsies. There were no CC-96673-related mortalities and no changes in body weight, food consumption, respiration rate, ophthalmic examinations, or ECGs that were considered test-article related. CC-96673 exposure increased in an approximately dose proportional manner in the range of 20 to 100 mg/kg on Day 1 and 60 to 100 mg/kg on Day 22 (Table S8). No accumulation was noted at the 60 mg/kg level, while at the 100 mg/kg dose level, CC-96673 accumulation ratios ranged from 1.3 to 1.5 in females and males (data not shown), respectively, suggesting modest time-dependent increases in systemic exposure after weekly dosing. ADA had profound impacts on exposure at the lowest dose of 20 mg/kg where all animals were ADA-positive with an approximately 82% decrease in total exposure (AUC$_{LST}$) from Day 1 to Day 22 dose, while the impact on exposure was lower at higher doses of 60 (all males and one female ADA-positive) and 100 mg/kg (one male and one female ADA-positive) (Table S8). IV administration of CC-99673 QW for 4 weeks resulted in expected pharmacologic decreases in B cells in peripheral blood and decreased cellularity in lymphoid organs at ≥20 mg/kg/dose. Infusion reactions considered secondary to ADA formation were noted at 20 mg/kg/dose on the final dose administration. Other ADA-related adverse effects were present in the kidneys and/or GI tract at ≥20 mg/kg/dose, with generally associated decreases in platelets and red cell mass. Minor decreases in red cell mass in the absence of other acute-phase changes were also present in individuals at 60 and 100 mg/kg/dose. Based on the expected but adverse pharmacological effects at all dose levels, a no observed adverse effect level (NOAEL) was not determined. Several toxic findings in the kidney at the 20 and 60 mg/kg/dose and a moderate-severe infusion reaction at the 20 mg/kg/dose were considered ADA-mediated and not a direct effect of CC-96673. Based on these results, 100 mg/kg administered once weekly was considered the highest non-severely toxic dose (HNSTD), corresponding
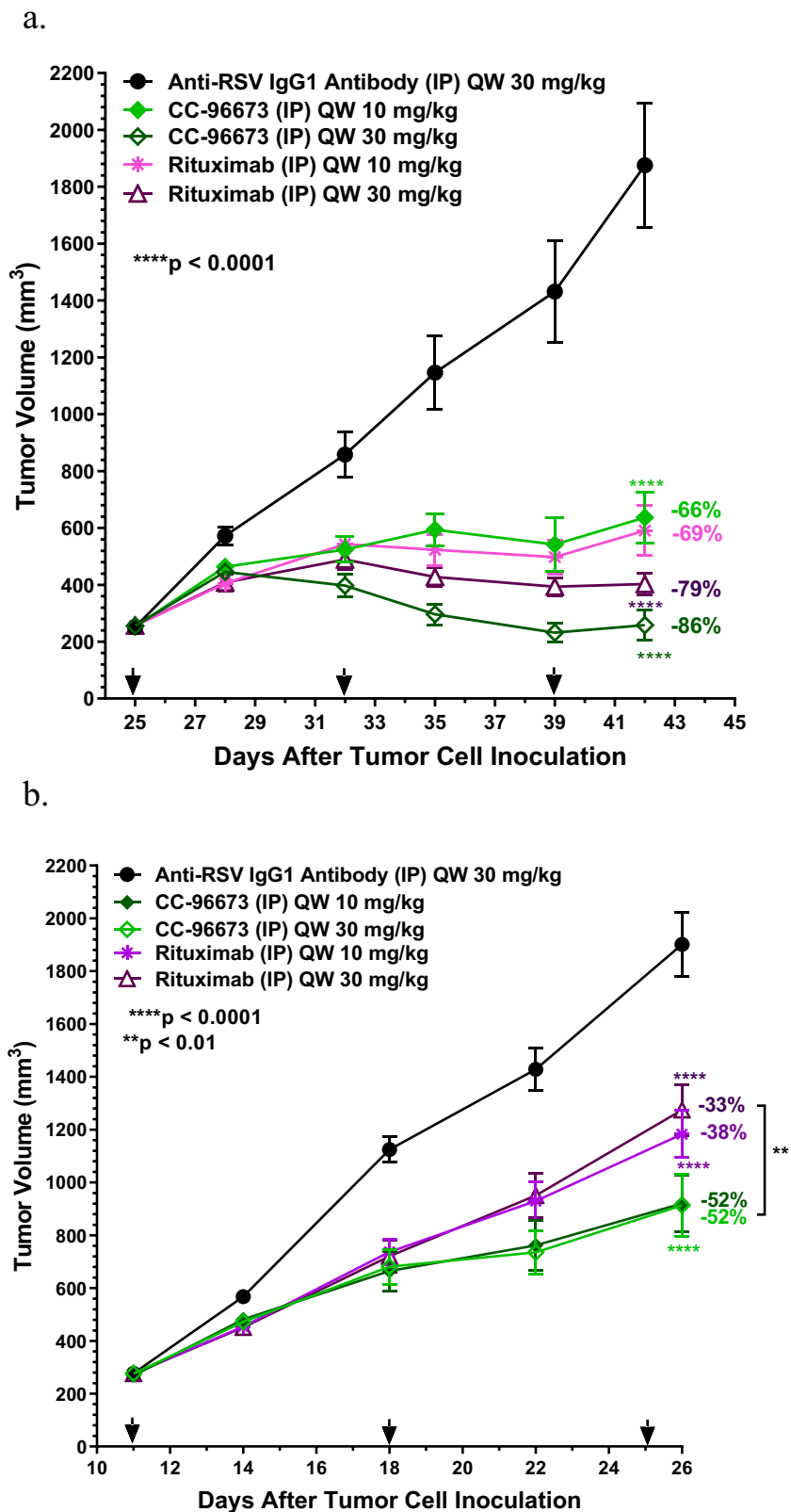
a.

b.

Figure 5. CC-96673 has antitumor activity in lymphoma xenograft models. (a) Tumor volume growth curves of WSU-DLCL2 or (b) Raji xenografts in female NOD-SCID mice treated with CC-96673, rituximab or the non-targeting anti-RSV IgG1. Mice were inoculated with 5×10^6 WSU-DLCL2 or 2×10^6 Raji tumor cells into the right flank and randomized into treatment groups ($n = 9$/group) at the time of treatment initiation. Test article treatment started on Day 25 or Day 11 when tumors were approximately 200 mm³. Tumor inhibition was calculated as the percentage difference in average tumor volume between CC-96673 and rituximab treated mice and anti-RSV IgG1 treated control mice on Day 42 (WSU-DLCL2) or Day 26 (Raji) and is shown to the right of the dose response curve for each treatment dose. Statistical analysis was performed using a two-way ANOVA with Bonferroni's multiple comparisons test with all the study groups, and the data shown are in comparison with the anti-RSV IgG1 control group. Values represent the mean ± SEM. Dosing days are indicated with arrows.

Table 1. Exposure parameters of CC-96673 following administration of a single intravenous dose or first intravenous dose of CC-96673 to cynomolgus monkeys in pharmacokinetic or toxicology studies.

IV Dose (mg/kg)	Mean SD	Cmax (µg/mL)	AUCLST (µg·hr/mL)	t½ (hr)	CL (mL/hr/kg)	Vd (mL/kg)
20 Single dose (n = 3)	Mean	608	69700	67	0.29	34.2
	SD	135	9190	18	0.04	5.9
10 (1st dose of RD) (n = 4)	Mean	146	5560	50	1.09	82.6
	SD	18.9	527	4.4	0.04	9.7
20 (1st dose of RD) (n = 4)	Mean	274	22700	110	0.56	92.2
	SD	8.2	2100	8.2	13.0	7.4
100 (1st dose of RD) (n = 4)	Mean	1330	91400	86	0.76	104
	SD	189	2880	5.7	0.03	4.9

AUCLST = area under the concentration–time curve calculated to the last observable concentration at time t; CL = clearance; Cmax = observed maximum concentration; hr = hour; IV = intravenous; RD = repeat dose; SD = standard deviation; t½, half-life; Vd = volume of distribution.

to a Day 22 AUC_{LST} of 312,000 µg.hr/mL and a Cmax of 4640 µg/mL (Table S8).

Discussion

The CD47-SIRPα axis plays a crucial role in immune recognition and prevention of macrophage attacks on healthy normal cells. Cancer cells often upregulate CD47 expression and transmit a "don't eat me" signal to macrophages by engaging the macrophage checkpoint inhibitor SIRPα, consequently evading the innate immune system. A growing number of studies have demonstrated that CD47 blocking antibodies enhance the phagocyte-mediated elimination of cancer cells, and a series of immuno-modulators targeting the CD47–SIRPα interaction have entered clinical development.[27] Still, the therapeutic utility of CD47-SIRPα blocking agents is severely challenged by substantial hematotoxicity and poor pharmacokinetics due to the widespread expression of CD47 on normal cells, including senescent RBCs. Various approaches have been used in preclinical research and in clinical studies to address these hurdles. A new generation of anti-CD47 antibodies that maintain the on-target on-tumor activity but decrease the on-target off-tumor binding to CD47 on normal cells have been reported.[19,28,45] Notably, the residual binding to CD47 by these next-generation anti-CD47 antibodies often necessitates the selection of Fc domains with reduced effector functions, such as IgG2[20] or IgG4,[21,28] to preserve normal cells. This limits the single-agent efficacy of anti-CD47 mAbs, not only because of the "antigen sink" preventing them from reaching tumor cells, but also due to the lack of pro-phagocytic signals that trigger macrophages via FcγR binding. Dual-targeting antibodies that bind CD47 and a selective tumor antigen are another strategy that has been explored to increase the therapeutic index of anti-CD47 agents in hematological malignancies. For example, a reduced affinity to CD47 was achieved by positioning the anti-CD47 variable domain into the internal position of a dual-variable domain immunoglobulin (DVD-Ig) molecule co-targeting CD47 and CD20, permitting preferential binding to dual antigen-positive cells.[32] Likewise, RTX-CD47, a CD20-targeted single-chain variable fragment (scFv) derived from rituximab fused in tandem to a CD47-blocking scFv,[30] was shown to promote a CD20-directed blockade of the CD47-SIRPα signal toward CD20 and CD47 expressing cancer cells and to augment the ADCP activity of therapeutic antibodies directed to B cell malignancies (e.g., obinutuzumab).[30] However, the inherent absence of an Fc domain with this scFv format may limit its single agent phagocytic activity *in vivo* due to a shortened half-life and a lack of activating FcγR signaling. Alternatively, zeripatamig (NI-1701), a κλ body BsAb comprising a high-affinity anti-CD19 targeting arm and an anti-CD47 arm with optimized low affinity in a human IgG1 Fc-competent backbone, selectively blocks the "don't eat me" signal on CD19$^+$ cells and induces tumor cell killing *in vitro* and *in vivo*.[34] It is being developed in Phase 1 for CD19-positive leukemias and lymphomas and may benefit patients who are resistant to CD20 mAbs. IMM0306, an immunoconjugate composed of a CD20-targeted mAb fused to the CD47 binding domain of SIRPα, was designed to have a higher affinity for CD20 than for CD47, thus enabling its preferential binding to CD20- and CD47-positive malignant B cells rather than to CD47-positive normal tissues. In Phase 1/2, it was well-tolerated with a preliminary anti-tumor activity in patients with R/R FL and MZL.[46]

Based on these findings and clinical data from current anti-CD47 therapeutics, we hypothesized that an IgG1 Zymeworks BsAb with a wild-type Fc domain, targeting CD20 and CD47, with detuned affinity to CD47 could achieve the following: 1) Retain efficacy in mediating anti-tumor function by targeting the CD47–SIRPα interaction and engaging activating FcγRs; 2) Minimize target-mediated sink effects and toxicity observed with anti-CD47 therapeutics; 3) Incorporate CD20 and CD47 engagement in a single molecule avoiding the need for combination therapy with two mAbs; 4) Preserve the native IgG format with the Zymeworks Azymetric pairings so as to minimize the drug development risks associated with non-traditional antibody formats (e.g., increased risk of immunogenicity, decreased stability, and reduced half-life). A functional cell-based screen was implemented to identify CD47 binders with affinities that are at the limit of avidity, thereby minimizing binding to CD47 alone and maximizing the possible inhibition of the CD47–SIRPa interaction via CD20-guided avidity-driven binding to the CD47 antigen. As a result, CC-96673 has been developed in a standard IgG-based BsAb format co-targeting CD47 and CD20, with high affinity to CD20 and an optimally detuned affinity to CD47, engineered with a human IgG1
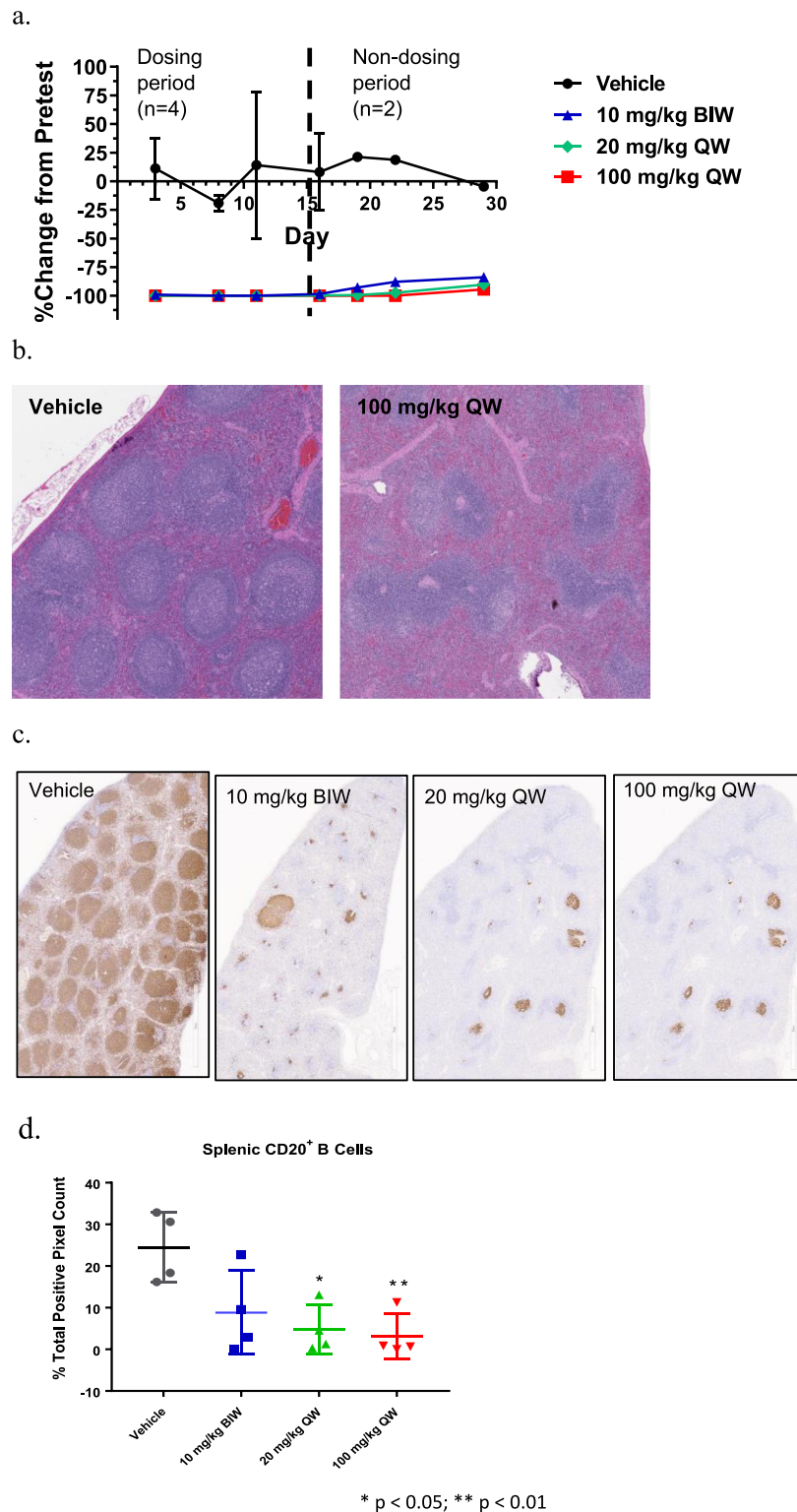
a.

b.

c.

d.

* p < 0.05; ** p < 0.01

Figure 6. CC-96673 induced robust decreases in B cells in cynomolgus monkeys. (a) CC-96673 decreased B lymphocytes in the peripheral blood of cynomolgus monkeys. Percentage B cells was assessed by immunophenotyping and flow cytometry using blood collected at predose and multiple timepoints postdose. (b) CC-96673 decreased B cells in multiple lymphoid tissues. Representative photomicrographs showing diminished lymphoid cellularity in the follicular (B cell) areas of the spleen as observed on Day 16 by hematoxylin and eosin stain. (c) Moderate to marked decreases in staining of B cells in the spleen by immunohistochemistry, consistent with decreased B cells in peripheral blood and with microscopic changes seen in lymphoid tissues. (d) Quantitation of the area of CD20+ stained cells in spleen, expressed as positive pixel counts. BIW = twice per week; QW = once per week; *$p < .05$, **$p < .01$.

backbone that contains Zymeworks Azymetric mutations to ensure its proper assembly. When bound to CD20-expressing cells, CC-96673 not only blocked the SIRPα interaction with CD47 but also engaged activating FcγRs to fully potentiate macrophages to engulf and destroy CD20-positive cells. Potent *in vitro* activity was induced by CC-96673 to eliminate cancer cells via multiple modes of action, including ADCP, ADCC, and CDC (Figure S6).

Several observations support the premise that CC-96673 provides enhanced pharmacological activities over rituximab or CC-90002, a non-detuned anti-CD47 antibody, and that its detuned CD47 arm contributes to immune effector function. Primarily, our CD47 × CD20 BsAb demonstrated enhanced phagocytosis compared to rituximab or single agent anti-CD47 mAbs and had equivalent phagocytic activity to the combination of CC-90002 and rituximab against the NHL cell line OCI-Ly3 (Figure 3). Furthermore, among our various lead CD47 × CD20 BsAbs with detuned CD47 arms, phagocytic potency was proportional to the affinity for the CD47 antigen (data not shown), indicating involvement of the CD47 binding arm. CC-96673 also displayed higher binding to several members of the Fcγ receptor family than rituximab, including FcγR3A expressed by NK cells, and induced a more potent ADCC in CD20$^+$ tumor cells than rituximab (Table S5 and Figure 4a). Likewise, the combined targeting of anti-CD20 and anti-CD47 resulted in the enhanced antitumor activity of CC-96673 over rituximab in a Raji NOD-SCID *in vivo* tumor model (Figure 5).

Consistent with its reduced affinity for the human and cynomolgus monkey CD47 protein, CC-96673 did not bind to human or cynomolgus monkey RBCs, even at high concentrations of up to 1333.3 nM, and did not induce human RBC agglutination (Figure 2 and Figure S2). It also did not induce cytokine release from human PBMCs tested in a plate-bound assay format (data not shown). As expected, CC-96673 administration in cynomolgus monkeys resulted in marked decreases in peripheral blood B cells, with associated decreased cellularity of lymphoid organs and minimal drug-related impacts on peripheral RBCs (Figure 6). Observed decreases in T cells, NK cells, and neutrophils may be due to FcγR binding and the consequent increased avidity to CD47, since NK cells and neutrophils do not express CD20, although there are recent reports of a subset of CD20$^+$ T cells. The safety profile of CD20 and CD47 targeting agents is well established, and the primary B cell depletion effects of CC-96673 in cynomolgus monkeys were consistent with known pharmacology and with the effects of other agents targeting CD20 or CD47. Such pharmacologic effects have been shown to be reversible in cynomolgus monkeys and/or patients treated with rituximab[47–50] or a rituximab biosimilar.[51] As B cell depletion in lymphoid tissues is not instantaneous, ADA was observed in CC-96673 dosed cynomolgus monkeys, which had an impact on CC-96673 exposure. These anti-drug antibody responses are observed in cynomolgus monkeys for other B-cell depleting agents and may be related to the persistence of B cells in lymphoid organs for a sufficient duration to generate an antibody response. Finally, with the total systemic CL predicted to be 0.366 mL/hr/kg and the total Vd predicted to be 63.28 mL/kg, the half-life for CC-96673 in humans is expected to be ~5 days.

Taken together, CC-96673, a humanized BsAb antibody co-targeting CD47 and CD20, exhibited potent macrophage-mediated phagocytosis by blocking the CD47–SIRPα interaction, and mediated ADCC and CDC to selectively eliminate CD20-expressing tumor cells, while alleviating the potential toxicity associated with global CD47 blockade. *In vivo*, CC-96673 significantly inhibited tumor growth in two lymphoma cell line xenograft models and was well-tolerated in non-human primates. The cumulative data presented here indicate the potential of CC-96673 to widen the safety margin of therapeutic CD47 targeting in patients, thus providing a rationale for clinical investigation of CC-96673 as a single agent and in combination with other cancer therapeutics in NHL patients who have progressed on standard of care. CC-96673 is being studied in a Phase 1 clinical trial (NCT04860466) in participants with relapsed or refractory NHL.

Materials and methods

Materials

All tumor cells were maintained according to vendors' protocols. Raji, SC-1, and REC-1 cells were obtained from ATCC. OCI-Ly3, WSU-FSCCL, WSU-DLCL2, and RIVA cells were obtained from DSMZ. All cells were grown in RPMI-1640 medium (ThermoFisher) supplemented with 10% heat-inactivated fetal bovine serum (FBS) (ThermoFisher, catalog number 16000044). Cells were subcultured for no more than 10 passes and tested for mycoplasma infection (Lonza) prior to cryopreservation.

RBCs were isolated from human whole blood from healthy volunteers obtained from The Scripps Research Institute Normal Blood Donor Service (La Jolla, CA, USA). Fresh human NK cells and neutrophils were isolated from human whole blood (BioIVT) using EasySep™ Direct Human NK or Neutrophil Cell Isolation Kits (Stem Cell Technologies). Frozen human PBMCs and NK cells were purchased from Astarte Biologics (Charles River Laboratories). Cynomolgus monkey RBCs were isolated from whole blood collected at pretest from cynomolgus monkeys from Envigo Study No. CY04WL.

The anti-RSV IgG1 antibody was expressed and purified in-house upon co-transfecting plasmids containing the VH and VL sequences of palivizumab with their respective IgG1 heavy and kappa light chain constant regions. The antibody was expressed in Chinese hamster ovary cells and purified via protein A affinity chromatography.

Affinity determination by surface plasmon resonance

Surface plasmon resonance (SPR) with a Biacore T200 and S200 spectrometer (Biacore AB) was used to evaluate CC-96673 kinetics of binding to recombinant human and cynomolgus monkey CD47 ECD proteins (Celgene Corporation, catalog numbers TPP-43 and TPP-2206 for human and cynomolgus monkey CD47 proteins, respectively). Binding was assessed over a wide concentration range (two-fold dilutions from 0.41 nM to 3750 nM) of monomeric human or cynomolgus monkey CD47. The resonance signal over a span of 300 s at each antigen concentration was captured, analyzed, and fitted with a 1:1 Langmuir model using the Biacore Evaluation software.

An assessment of CC-96673 binding to human CD20 full-length protein was also performed by SPR. His-tagged human CD20 antigen (Acro Biosystems, catalog number CD0-H52H3) was captured at a fixed concentration (2.5 μg/mL) by immobilized anti-His antibody (Cytiva, catalog number 28995056) on the surface of a Series S Sensor Chip CM5. 1X HBS-EP running buffer with 0.05% n-Dodecyl-beta-Maltoside Detergent (DDM) (Thermo Fisher, catalog number 89902) and 0.01% Cholesteryl Hemisuccinate Tris Salt (CHS)

(Sigma, catalog number 013-5 G) was used to keep the CD20 protein soluble and active. Binding of CC-96673 and rituximab was assessed over a wide concentration range (two-fold dilutions from 1000 nM to 3.9 nM). The resonance signal over a span of 120 s at each antibody concentration was captured, analyzed, and fitted with a steady state model using the Biacore Evaluation software.

CD47-SIRPα blocking analysis by flow cytometry

The surface expression of CD47 and CD20 on NHL cell lines was determined prior to the assessment of SIRPα binding competition using the Quantum Simply Cellular (QSC) anti-human IgG kit (Bangs Laboratories), as per the manufacturer's instructions. The potency of CC-96673 to block human SIRPα binding to human CD47 on tumor cells was assessed using flow cytometry. Cells were seeded into 96-well plates, blocked with Human BD Fc Block (BD Pharmingen), and incubated with CC-96673, anti-RSV IgG1 (Bristol Myers Squibb), TPP-23, or Stain Buffer (BD Pharmingen) alone for 30 min at room temperature. Cell pellets were then mixed with a preformed complex of human SIRPα protein (Abcam, catalog number ab221342) and Alexa Fluor 647 (AF647) goat anti-mouse IgG, Fcγ-specific (Jackson ImmunoResearch, catalog number 115-605-071) and further incubated at 4°C for 30 min. All the samples were fixed with 1% paraformaldehyde prior to analysis on a BD FACSCanto II flow cytometer (BD Biosciences). Blocking IC_{50} and maximum percent inhibition were calculated for each tumor cell line, with the geometric mean fluorescence intensity (gMFI) values from Stain Buffer only wells serving as 100%.

Cellular binding

For binding to human immune cell subsets isolated from whole blood or PBMCs, CC-96673 and control antibodies were prelabeled with AF647 using the Alexa Fluor 647 Antibody Labeling Kit (ThermoFisher), according to manufacturer's instructions. AF647-labeled test antibodies were added to individual tubes of a master surface stain mix (Table S9) for a final concentration of 200 nM. Whole blood or purified PBMCs were added to round-bottom 96-well plates at 200 uL/well and stained with 50 uL stain mix at 4°C for 30 min, fixed with 1% paraformaldehyde, and analyzed on a BD FACSFortessa flow cytometer (BD Biosciences). Fluorescent minus one (FMO) control wells were included. Compensation was set up using single-color stained UltraComp eBeads (ThermoFisher) and BD FACSDiva software. Cryopreserved human PBMCs were seeded at 1×10^6 cells/well in a round-bottom 96-well plate and blocked in 1:20 Human BD Fc Block in Stain Buffer for 10 min at room temperature, prior to staining and analysis as detailed above.

For binding to purified human or cynomolgus monkey RBCs, cells were incubated with unlabeled test antibodies followed by staining with an AF647 goat anti-human IgG (H+L) Fab Fragment (Jackson ImmunoResearch, catalog number 115-606-071). Human whole blood was processed within 2 h of delivery by centrifugation of 10 mL at 500 × g for 10 min, break off. The top layer of platelet-rich plasma was carefully aspirated, and the RBC pellet washed twice in 50 mL Dulbecco's phosphate-buffered saline (DPBS). For cynomolgus monkey whole blood samples, 1 mL of each sample was diluted with 1 mL of DPBS and layered onto 1.5 mL Histopaque-1077 (Millipore-Sigma) before centrifugation at 400 × g for 30 min, break off. The top layers of plasma and mononuclear cells were carefully aspirated, and the RBC pellet washed twice in 10 ml DPBS.

To determine whether CC-96673 could selectively bind dual antigen-expressing cells in the presence of excess CD47-only expressing cells, CC-96673 was incubated with mixtures of Fc-blocked human RBCs (CD47+) and Raji tumor cells (CD47+CD20+) for 30 min at room temperature. Cell pellets were then processed for flow cytometry using an AF647-secondary antibody, as above.

Hemagglutination assay

To evaluate the hemagglutinating capacity of CC-96673, human RBCs were diluted to 10% in DPBS and incubated at 37°C overnight with a titration of anti-CD47 antibodies in round-bottom 96-well plates. Evidence of hemagglutination was demonstrated by the presence of non-settled RBCs, appearing as a haze compared to the punctate red dot of non-hemagglutinated RBCs.

Phagocytosis, ADCC, and CDC

Macrophages were generated by incubating purified normal human peripheral blood monocytes in AIM-V medium (ThermoFisher) containing 50 ng/mL M-CSF and 10% FBS, for 6–10 days in black-walled 96-well PhenoPlates (Perkin Elmer), at a density of 40,000 cells/well. To measure phagocytosis, NHL cells were labeled with carboxyfluorescein diacetate succinimidyl ester (CFSE), plated at 40,000 cells/well, and opsonized with CC-96673 or control antibodies, including rituximab and anti-RSV IgG1. Tumor cells were added to macrophages pre-incubated with equal concentrations of the same antibodies. After 3 h at 37°C, cells were stained with an Allophycocyanin (APC) anti-human CD14 antibody (BioLegend, catalog number 365608) to label macrophages, and the plate was imaged using an Operetta CLS High-Content Analysis System (Perkin Elmer). Harmony analysis software was applied to count the number of APC-positive and CFSE/APC-double positive cells and to determine percent phagocytosis (the number of double-positive cells divided by the total number of APC-positive cells). Each assay condition was tested in triplicate with three repeats per donor.

CC-96673-mediated ADCC directed against cells expressing CD47 and CD20 was assessed using Raji, OCI-Ly3, SC-1, and WSU-FSCCL cells as targets and purified human NK cells from two donors as effectors. NK cells were mixed with tumor cells labeled with CellTrace Violet (Invitrogen) at a ratio of 10:1 in RPMI 1640 containing 5% FBS and incubated with antibodies for 4 h at 37°C. Each antibody concentration was assayed in triplicate wells. Rituximab treated cells were used as a positive control; anti-RSV IgG1 was used as a negative control. Cell lysis was determined using propidium iodide and flow cytometry with a BD FACSCelesta

(BD Biosciences). Percent increase in ADCC was calculated as follows: % ADCC = (% cell death in the presence of IgG - % cell death in the absence of IgG)/(% Cell death with maximum lysis - % cell death in the absence of IgG) × 100. Maximum lysis was obtained using Triton X-100 at a final concentration of 5%.

CDC assays were performed by incubating REC-1 cells with CC-96673 or rituximab for 30 min at 37°C, before adding diluted rabbit serum as a source of complement and incubating for further 2 h at 37°C. Cell viability was assessed using the CellTiter-Glo Luminescent Cell Viability Assay (Promega) on an EnVision XCite plate reader (Perkin Elmer). Cell viability under treatment was normalized with cell viability in the presence of negative control, anti-RSV IgG1.

Ex vivo autologous human B cell depletion

CC-96673-mediated autologous human B cell depletion was assessed using a flow cytometry-based assay. Whole blood from 12 healthy donors was diluted 1:1 with serum-free RPMI 1640 and 600 uL incubated with 50 uL CC-96673 or control antibodies for 24 h at 37°C. The mixture was then blocked with Human TruStain FcX Receptor Block (BioLegend) and stained with fluorescently labeled anti-human CD45 (lymphocyte population) (BioLegend, catalog number 368518), CD3 (T cells) (BioLegend, catalog number 300322), and CD19 (BioLegend, catalog number 302234), or CD79b (B cells) (BioLegend, catalog number 341404) antibodies for 30 min at 4°C. FMO control wells were included. RBCs were lysed in 2X RBC Lysis Buffer (BioLegend) for 20 min at 37°C and remaining PBMCs fixed with FluoroFix Buffer (BioLegend) at room temperature for 30 min. B and T cell counts were determined by flow cytometry using a BD FACSCanto II (BD Biosciences). All assays included rituximab as a positive control and anti-RSV IgG1 as a negative control, and conditions were tested in triplicate wells. Relative B cell depletion was calculated as follows: B/T cell ratio = B cell count/T cell count within the CD45-positive lymphocyte gate; % remaining B cells = 100 × [(B/T treated with IgG)/(B/T no IgG treatment)], using untreated samples as the 100% control.

Surplus blood from each donor was also used to isolate PBMCs for evaluation of cell surface CD47, CD20, and CD19 using the microsphere-based QSC assay (Bangs Laboratories), as per the manufacturer's instructions.

FCGR SNP genotyping

The FCGR2A 131 R/H SNP (rs1801274) and FCGR3A 158 V/F SNP (rs396991) status of donor whole blood was analyzed using TaqMan SNP Genotyping Assays (ThermoFisher). Genomic DNA was isolated from PBMCs using the QIAamp Blood DNA Mini Kit (Qiagen) and 4 ng/uL added to each SNP assay in TaqMan Genotyping Mastermix (ThermoFisher). Thermo-cycling was performed as per the manufacturer's instructions using a QuantStudio 7 Flex Real-Time PCR system (ThermoFisher), with inclusion of an endpoint plate read.

Post-PCR allelic discrimination was performed using QuantStudio7 v.3 software (ThermoFisher).

In vivo tumor studies

All animal studies were conducted according to guidelines established by the internal Institutional Animal Care and Use Committee (IACUC). Female NOD-SCID mice were inoculated subcutaneously with Raji or WSU-DLCL2 tumor cells as a single-cell suspension containing 50% Matrigel (Corning). Animals with tumors of approximately 200 mm^3 were randomly assigned to treatment groups. CC-96673 and anti-RSV IgG1 were formulated in 9% sucrose in 10 mM Sodium Acetate (pH 5.2); rituximab was formulated in saline. Tumor volumes were calculated using the formula: width^2 × length/2 and expressed in mm.^{3} Percent body weight change during the study was calculated based off initial body weight measurements.

Non-human primate pharmacokinetics and toxicity studies

Single- and repeated-dose pharmacokinetic and toxicity studies were conducted at Charles River Laboratories (Reno, NV, USA) and Covance CRS, LLC (Somerset, NJ, USA), respectively, each according to a written study protocol and facility standard operating procedures in compliance with IACUC criteria, national legal regulations on animal welfare, and accepted animal welfare standards. One repeat-dose study was conducted in compliance with the Food and Drug Administration (FDA) Good Laboratory Practice Regulations (GLP) as set forth in Title 21 of the US Code of Federal Regulations, Part 58. For the single-dose pharmacokinetic study, naive female cynomolgus monkeys (three animals per dose) were administered a single IV infusion of CC-96673 (20 mg/kg) or vehicle control (10 mM sodium acetate, 9% sucrose [w/v], 0.005% polysorbate 80 [w/v], pH 5.2) and samples were collected for PK analysis at predose, 0.25, 1, 4, 24, 72, 168, 240, and 336 h postdose. In one repeat-dose toxicity study, CC-96673 was administered by IV bolus injection to naive cynomolgus monkeys (two animals/sex/group) at dosage levels of 0 (10 mM sodium acetate, 9% sucrose [w/v], 0.005% polysorbate 80 [w/v], pH 5.2), 20, or 100 mg/kg QW on Days 1, 8, and 15 or at a dosage level of 10 mg/kg BIW on Days 1, 4, 8, 11, and 15. One animal per sex from each group was sacrificed and necropsied at the end of dosing on Day 16 and the remaining animals were sacrificed and necropsied on Day 29, following a 14-day non-dosing period. Parameters evaluated during the study were as follows: viability, clinical observations, body weight, body temperature, clinical pathology, immunophenotyping of peripheral blood lymphocytes, toxicokinetics, immunogenicity/ADA, gross pathology, and histopathology.

Immunophenotyping of whole blood from all animals was performed by the testing facility's Immunology and Immunotoxicology (I&I) department using a scientifically sound but not validated flow cytometry method. Samples were prepared using antibodies to CD3, CD159a, CD14, CD4, CD20, CD45, and CD8 and acquired on the BD FACSCanto II flow cytometer (BD Biosciences). Immune cell percentages were enumerated as

percentages relative to parent populations and reported directly from the flow cytometer. Absolute cell counts (cells/μL) were determined via a dual platform approach using lymphocyte counts from the ADVIA 120 Hematology Analyzer (Siemens). Data were analyzed as percentages and absolute counts of Total T cells ($CD45^+CD14^-CD3^+CD20^-$), Helper T cells ($CD45^+CD14^-CD3^+CD4^+$), Cytotoxic T cells ($CD45^+CD14^-CD3^+CD8^+$), B cells ($CD45^+CD14^-CD3^-CD20^+$) and NK cells ($CD45^+CD14^-CD3^-CD20^-CD159a^+$) in whole blood. Since the test articles and the anti-CD20 clone L27 mAb utilized for B cell detection bind to a similar epitope, data were also re-analyzed using a different gating strategy where B cells were defined as $CD45^+CD14^-CD3^-CD159a^-\,CD8^-$.

Immunohistochemistry of spleens was performed on the Bond Rx automated slide stainer (Leica Biosystems) using the associated Bond detection protocol: 4-μm-thick sections were deparaffinized, and antigen retrieval was performed with Epitope Retrieval Solution 2 (ER2, pH 9.0) for 20 min at 100°C. The sections were blocked for endogenous peroxidase activity with Peroxide Block for 5 min at room temperature and incubated with the primary antibody (Novocastra™ Mouse Monoclonal Anti-CD20 clone L26) at 1/1000 dilution for 30 min at room temperature. Horseradish peroxidase-labeled polymer was used at the instrument's default conditions. The antigen–antibody complex was then visualized with hydrogen peroxide substrate and diaminobenzidine tetrahydrochloride (DAB) chromogen. Slides were counterstained with hematoxylin, dehydrated, and coverslipped by the Tissue-Tek Film® Automated Coverslipper.

Estimation of B cells was done by quantification of CD20-positive pixels from digital images using an algorithm that relies on the quantification of the area positively stained and is expressed as percent positive pixel count.

In a repeat-dose GLP-compliant toxicity study, CC-96673 was administered weekly (Days 1, 8, 15, 22, and 29) at 20, 60, and 100 mg/kg QW (three animals/sex/group). In-life sampling, monitoring, and/or evaluations included clinical observations, body weight, food consumption, cardiovascular safety pharmacology (repeat-dose study only), clinical pathology, and toxicokinetics and ADA analysis. At the end of the treatment period (Day 29), animals were euthanized, necropsied, and subjected to a complete histopathology evaluation.

Graphical representation, curve fitting, and statistical analysis

The dose–response curves were fitted by non-linear regression with a variable slope (four parameters) in GraphPad Prism 10. EC_{50} or IC_{50} values were calculated in GraphPad Prism as the concentration that gives a response halfway between the bottom and top of the curve. Statistical testing was performed in GraphPad Prism 10 as indicated in the figure legends.

Notes on attributors

DZ wrote the manuscript with input from all authors. HH, KH, DZ, HC contributed to the conception and development of the project. DM, CJ, and JL performed experiments and analyzed data. SA and JL generated antibodies and recombinant proteins. RKN and AM coordinated *in vivo* mouse studies and data analysis. JP and KS coordinated the cyno studies and data analyses. All authors read and approved the final version of the manuscript.

Abbreviations

ADCC	antibody-dependent cellular cytotoxicity
ADCP	antibody-dependent cellular phagocytosis
CD	cluster of differentiation
CDC	complement-dependent cytotoxicity
FcγR	fragment crystallizable gamma receptor
IgG	immunoglobulin G
SIRPα	signal-regulatory protein alpha
VH	immunoglobulin heavy chain variable region
VL	immunoglobulin light chain variable region

References

1. Chao MP, Weissman IL, Majeti R. The CD47-SIRPalpha pathway in cancer immune evasion and potential therapeutic implications. Curr Opin Immunol. 2012;24:225–32. doi:10.1016/j.coi.2012.01.010. PMID: 22310103.
2. Taylor PR, Martinez-Pomares L, Stacey M, Lin HH, Brown GD, Gordon S. Macrophage receptors and immune recognition. Annu Rev Immunol. 2005;23:901–44. doi:10.1146/annurev.immunol.23.021704.115816. PMID: 15771589.
3. Matozaki T, Murata Y, Okazawa H, Ohnishi H. Functions and molecular mechanisms of the CD47–SIRPα signalling pathway. Trends Cell Biol. 2009;19(2):72–80. doi: 10.1016/j.tcb.2008.12.001. PMID: 19144521.
4. Fujioka Y, Matozaki T, Noguchi T, Iwamatsu A, Yamao T, Takahashi N, Tsuda M, Takada T, Kasuga M. A novel membrane glycoprotein, SHPS-1, that binds the SH2-domain-containing protein tyrosine phosphatase SHP-2 in response to mitogens and cell adhesion. Mol Cell Biol. 1996;16:6887–99. doi:10.1128/MCB.16.12.6887. PMID: 8943344.
5. Russ A, Hua AB, Montfort WR, Rahman B, Riaz IB, Khalid MU, Carew JS, Nawrocki ST, Persky D, Anwer F. Blocking "don't eat me" signal of CD47-SIRPalpha in hematological malignancies, an in-depth review. Blood Rev. 2018;32:480–89. doi:10.1016/j.blre.2018.04.005. PMID: 29709247.
6. Matlung HL, Szilagyi K, Barclay NA, van den Berg TK. The CD47-SIRPalpha signaling axis as an innate immune checkpoint in cancer. Immunol Rev. 2017;276:145–64. doi:10.1111/imr.12527. PMID: 28258703.
7. Majeti R, Chao MP, Alizadeh AA, Pang WW, Jaiswal S, Gibbs KD Jr., van Rooijen N, Weissman IL. CD47 is an adverse prognostic factor and therapeutic antibody target on human acute myeloid

leukemia stem cells. Cell. 2009;138:286–99. doi:10.1016/j.cell.2009.05.045. PMID: 19632179.

8. Galli S, Zlobec I, Schurch C, Perren A, Ochsenbein AF, Banz Y. CD47 protein expression in acute myeloid leukemia: a tissue microarray-based analysis. Leuk Res. 2015;39:749–56. doi:10.1016/j.leukres.2015.04.007. PMID: 25943033.

9. Willingham SB, Volkmer JP, Gentles AJ, Sahoo D, Dalerba P, Mitra SS, Wang J, Contreras-Trujillo H, Martin R, Cohen JD. et al. The CD47-signal regulatory protein alpha (SIRPa) interaction is a therapeutic target for human solid tumors. Proc Natl Acad Sci U S A. 2012;109:6662–67. doi:10.1073/pnas.1121623109. PMID: 22451913.

10. Yoshida K, Tsujimoto H, Matsumura K, Kinoshita M, Takahata R, Matsumoto Y, Hiraki S, Ono S, Seki S, Yamamoto J. et al. CD47 is an adverse prognostic factor and a therapeutic target in gastric cancer. Cancer Med. 2015;4:1322–33. doi:10.1002/cam4.478. PMID: 26077800.

11. Yuan J, He H, Chen C, Wu J, Rao J, Yan H. Combined high expression of CD47 and CD68 is a novel prognostic factor for breast cancer patients. Cancer Cell Int. 2019;19:238. doi:10.1186/s12935-019-0957-0. PMID: 31528120.

12. Liu J, Wang L, Zhao F, Tseng S, Narayanan C, Shura L, Willingham S, Howard M, Prohaska S, Volkmer J. et al. Pre-clinical development of a humanized anti-CD47 antibody with anti-cancer therapeutic potential. PloS ONE. 2015;10:e0137345. doi:10.1371/journal.pone.0137345. PMID: 26390038.

13. Weiskopf K, Jahchan NS, Schnorr PJ, Cristea S, Ring AM, Maute RL, Volkmer AK, Volkmer JP, Liu J, Lim JS. et al. CD47-blocking immunotherapies stimulate macrophage-mediated destruction of small-cell lung cancer. J Clin Invest. 2016;126:2610–20. doi:10.1172/JCI81603. PMID: 27294525.

14. Ring NG, Herndler-Brandstetter D, Weiskopf K, Shan L, Volkmer JP, George BM, Lietzenmayer M, McKenna KM, Naik TJ, McCarty A. et al. Anti-SIRPalpha antibody immunotherapy enhances neutrophil and macrophage antitumor activity. Proc Natl Acad Sci U S A. 2017;114:E10578–85. doi:10.1073/pnas.1710877114. PMID: 29158380.

15. Petrova PS, Viller NN, Wong M, Pang X, Lin GH, Dodge K, Chai V, Chen H, Lee V, House V. et al. TTI-621 (SIRPalphaFc): a CD47-blocking innate immune checkpoint inhibitor with broad antitumor activity and minimal erythrocyte binding. Clin Cancer Res. 2017;23:1068–79. doi:10.1158/1078-0432.CCR-16-1700. PMID: 27856600.

16. Uno S, Kinoshita Y, Azuma Y, Tsunenari T, Yoshimura Y, Iida S, Kikuchi Y, Yamada-Okabe H, Fukushima N. Antitumor activity of a monoclonal antibody against CD47 in xenograft models of human leukemia. Oncol Rep. 2007;17:1189–1194. https://www.ncbi.nlm.nih.gov/pubmed/17390064. PMID: 17390064.

17. Murata Y, Saito Y, Kotani T, Matozaki T. CD47-signal regulatory protein alpha signaling system and its application to cancer immunotherapy. Cancer Sci. 2018;109:2349–57. doi:10.1111/cas.13663. PMID: 29873856.

18. Peluso MO, Adam A, Armet CM, Zhang L, O'Connor RW, Lee BH, Lake AC, Normant E, Chappel SC, Hill JA. et al. The fully human anti-CD47 antibody SRF231 exerts dual-mechanism antitumor activity via engagement of the activating receptor CD32a. J Immunother Cancer. 2020;8(1):e000413. doi:10.1136/jitc-2019-000413. PMID: 32345627.

19. Puro RJ, Bouchlaka MN, Hiebsch RR, Capoccia BJ, Donio MJ, Manning PT, Frazier WA, Karr RW, Pereira DS. Development of AO-176, a next-generation humanized anti-CD47 antibody with novel anticancer properties and negligible red blood cell binding. Mol Cancer Ther. 2020;19:835–46. doi:10.1158/1535-7163.MCT-19-1079. PMID: 31879362.

20. Lin GHY, Chai V, Lee V, Dodge K, Truong T, Wong M, Johnson LD, Linderoth E, Pang X, Winston J. et al. TTI-621 (SIRPalphaFc), a CD47-blocking cancer immunotherapeutic, triggers phagocytosis of lymphoma cells by multiple polarized macrophage subsets. PloS ONE. 2017;12:e0187262. doi:10.1371/journal.pone.0187262. PMID: 29084248.

21. Narla RK, Modi H, Bauer D, Abbasian M, Leisten J, Piccotti JR, Kopytek S, Eckelman BP, Deveraux Q, Timmer J. et al. Modulation of CD47-SIRPalpha innate immune checkpoint axis with Fc-function detuned anti-CD47 therapeutic antibody. Cancer Immunol Immunother. 2022;71:473–89. doi:10.1007/s00262-021-03010-6. PMID: 34247273.

22. Veillette A, Tang Z. Signaling regulatory protein (Sirp)alpha-CD47 blockade joins the ranks of immune checkpoint inhibition. J Clin Oncol. 2019;37:1012–14. doi:10.1200/JCO.19.00121. PMID: 30811295.

23. Sikic BI, Lakhani N, Patnaik A, Shah SA, Chandana SR, Rasco D, Colevas AD, O'Rourke T, Narayanan S, Papadopoulos K. et al. First-in-human, first-in-class phase I trial of the anti-CD47 antibody Hu5F9-G4 in patients with advanced cancers. J Clin Oncol. 2019;37:946–53. doi:10.1200/JCO.18.02018. PMID: 30811285.

24. Ansell SM, Maris MB, Lesokhin AM, Chen RW, Flinn IW, Sawas A, Minden MD, Villa D, Percival MM, Advani AS. et al. Phase I study of the CD47 blocker TTI-621 in patients with relapsed or refractory hematologic malignancies. Clin Cancer Res. 2021;27:2190–99. doi:10.1158/1078-0432.CCR-20-3706. PMID: 33451977.

25. Zeidan AM, DeAngelo DJ, Palmer J, Seet CS, Tallman MS, Wei X, Raymon H, Sriraman P, Kopytek S, Bewersdorf JP. et al. Phase 1 study of anti-CD47 monoclonal antibody CC-90002 in patients with relapsed/refractory acute myeloid leukemia and high-risk myelodysplastic syndromes. Ann Hematol. 2022;101:557–69. doi:10.1007/s00277-021-04734-2. PMID: 34981142.

26. Oldenborg PA, Zhelezynak A, Fang YF, Lagenaur CF, Gresham HD, Lindberg FP. Role of CD47 as a marker of self on red blood cells. Sci. 2000;288(5473):2051–54. doi: 10.1126/science.288.5473.2051. PMID: 10856220.

27. Olaoba OT, Ayinde KS, Lateef OM, Akintubosun MO, Lawal KA, Adelusi TI. Is the new angel better than the old devil? Challenges and opportunities in CD47- SIRPalpha-based cancer therapy. Crit Rev Oncol Hematol. 2023;184:103939. doi:10.1016/j.critrevonc.2023.103939. PMID: 36774991.

28. Thaker YR, Rivera I, Pedros C, Singh AR, Rivero-Nava L, Zhou H, Swanson BA, Kerwin L, Zhang Y, Gray JD. et al. A novel affinity engineered anti-CD47 antibody with improved therapeutic index that preserves erythrocytes and normal immune cells. Front Oncol. 2022;12:884196. doi:10.3389/fonc.2022.884196. PMID: 35664753.

29. Ma L, Zhu M, Gai J, Li G, Chang Q, Qiao P, Cao L, Chen W, Zhang S, Wan Y. Preclinical development of a novel CD47 nano-body with less toxicity and enhanced anti-cancer therapeutic potential. J Nanobiotechnology. 2020;18:12. doi:10.1186/s12951-020-0571-2. PMID: 31931812.

30. van Bommel PE, He Y, Schepel I, Hendriks M, Wiersma VR, van Ginkel RJ, van Meerten T, Ammatuna E, Huls G, Samplonius DF. et al. CD20-selective inhibition of CD47-SIRPα "don't eat me" signaling with a bispecific antibody-derivative enhances the anticancer activity of daratumumab, alemtuzumab and obinutuzumab. Oncoimmunology. 2018;7:e1386361. doi:10.1080/2162402X.2017.1386361. PMID: 29308308.

31. Zhang B, Li W, Fan D, Tian W, Zhou J, Ji Z, Song Y. Advances in the study of CD47-based bispecific antibody in cancer immunotherapy. Immunology. 2022;167:15–27. doi:10.1111/imm.13498. PMID: 35575882.

32. Piccione EC, Juarez S, Liu J, Tseng S, Ryan CE, Narayanan C, Wang L, Weiskopf K, Majeti R. A bispecific antibody targeting CD47 and CD20 selectively binds and eliminates dual antigen expressing lymphoma cells. MAbs. 2015;7:946–56. doi:10.1080/19420862.2015.1062192. PMID: 26083076.

33. Dheilly E, Moine V, Broyer L, Salgado-Pires S, Johnson Z, Papaioannou A, Cons L, Calloud S, Majocchi S, Nelson R. et al. Selective blockade of the Ubiquitous checkpoint receptor CD47 is enabled by dual-targeting bispecific antibodies. Mol Ther. 2017;25:523–33. doi:10.1016/j.ymthe.2016.11.006. PMID: 28153099.

34. Buatois V, Johnson Z, Salgado-Pires S, Papaioannou A, Hatterer E, Chauchet X, Richard F, Barba L, Daubeuf B, Cons L. et al. Preclinical development of a bispecific antibody that safely and effectively targets CD19 and CD47 for the treatment of B-Cell Lymphoma and leukemia. Mol Cancer Ther. 2018;17:1739–51. doi:10.1158/1535-7163.MCT-17-1095. PMID: 29743205.

35. Jiang Z, Sun H, Yu J, Tian W, Song Y. Targeting CD47 for cancer immunotherapy. J Hematol Oncol. 2021;14:180. doi:10.1186/s13045-021-01197-w. PMID: 34717705.

36. Chao MP, Alizadeh AA, Tang C, Myklebust JH, Varghese B, Gill S, Jan M, Cha AC, Chan CK, Tan BT. et al. Anti-CD47 antibody synergizes with rituximab to promote phagocytosis and eradicate non-Hodgkin lymphoma. Cell. 2010;142:699–713. doi:10.1016/j.cell.2010.07.044. PMID: 20813259.

37. Weiskopf K, Ring AM, Ho CC, Volkmer JP, Levin AM, Volkmer AK, Ozkan E, Fernhoff NB, van de Rijn M, Weissman IL. et al. Engineered SIRPalpha variants as immunotherapeutic adjuvants to anticancer antibodies. Sci. 2013;341:88–91. doi:10.1126/science.1238856. PMID: 23722425.

38. Advani R, Flinn I, Popplewell L, Forero A, Bartlett NL, Ghosh N, Kline J, Roschewski M, LaCasce A, Collins GP. et al. CD47 blockade by Hu5F9-G4 and Rituximab in non-Hodgkin's lymphoma. N Engl J Med. 2018;379:1711–21. doi:10.1056/NEJMoa1807315. PMID: 30380386.

39. Hatterer E, Barba L, Noraz N, Daubeuf B, Aubry-Lachainaye JP, von der Weid B, Richard F, Kosco-Vilbois M, Ferlin W, Shang L. et al. Co-engaging CD47 and CD19 with a bispecific antibody abrogates B-cell receptor/CD19 association leading to impaired B-cell proliferation. MAbs. 2019;11:322–34. doi:10.1080/19420862.2018.1558698. PMID: 30569825.

40. Von Kreudenstein TS, Escobar-Carbrera E, Lario PI, D'Angelo I, Brault K, Kelly J, Durocher Y, Baardsnes J, Woods RJ, Xie MH. et al. Improving biophysical properties of a bispecific antibody scaffold to aid developability: quality by molecular design. MAbs. 2013;5:646–54. doi:10.4161/mabs.25632. PMID: 23924797.

41. Molecule Operating Environment (MOE). [Software] 2022.02 chemical computing group ULC, 910-1010 Sherbrooke St. W., Montreal, QC H3A 2R7, Canada; 2023. https://www.chemcomp.com/Research-Citing_MOE.htm.

42. Jawa V, Terry F, Gokemeijer J, Mitra-Kaushik S, Roberts BJ, Tourdot S, De Groot AS. T-Cell dependent immunogenicity of protein therapeutics pre-clinical assessment and mitigation-updated Consensus and review 2020. Front Immunol. 2020;11:1301. doi:10.3389/fimmu.2020.01301. PMID: 32695107.

43. Leclair P, Liu CC, Monajemi M, Reid GS, Sly LM, Lim CJ. CD47-ligation induced cell death in T-acute lymphoblastic leukemia. Cell Death Disease. 2018;9:544. doi:10.1038/s41419-018-0601-2. PMID: 29748606.

44. Leclair P, Lim CJ. CD47 (cluster of differentiation 47): an anti-phagocytic receptor with a multitude of signaling functions. Anim Cells Syst (Seoul). 2020;24:243–52. doi:10.1080/19768354.2020.1818618. PMID: 33224442.

45. Cao A, Yi J, Tang X, Szeto CW, Wu R, Wan B, Fang X, Li S, Wang L, Wang L. et al. CD47-blocking antibody ZL-1201 promotes tumor-associated macrophage phagocytic activity and enhances the efficacy of the therapeutic antibodies and chemotherapy. Cancer Res Commun. 2022;2:1404–17. doi:10.1158/2767-9764.CRC-22-0266. PMID: 36970051.

46. Yang J, Song Y, Li Z, Zhang M, Zhou K, Wang Z, Jing H, Yu L, Ma H, Zhao X. et al. Preliminary results from a phase I/II study of IMM0306, a CD47 and CD20 bispecific monoclonal antibody-trap, in patients with relapsed or refractory CD20-positive B-cell non-Hodgkin's lymphoma. J Clin Oncol. 2023;41:7527–7527. doi:10.1200/JCO.2023.41.16_suppl.7527.

47. Vulto AG. Biologicals and biosimilars in hematology: the case of Rituximab. Hemasphere. 2019;3:e322. doi:10.1097/HS9.0000000000000322. PMID: 31976491.

48. Enqvist M, Jacobs B, Junlen HR, Schaffer M, Melen CM, Friberg D, Wahlin BE, Malmberg KJ. Systemic and intra-nodal activation of NK cells after rituximab monotherapy for Follicular Lymphoma. Front Immunol. 2019;10:2085. doi:10.3389/fimmu.2019.02085. PMID: 31572357.

49. Berinstein NL, Grillo-Lopez AJ, White CA, Bence-Bruckler I, Maloney D, Czuczman M, Green D, Rosenberg J, McLaughlin P, Shen D. Association of serum Rituximab (IDEC-C2B8) concentration and anti-tumor response in the treatment of recurrent low-grade or follicular non-Hodgkin's lymphoma. Ann Oncol. 1998;9:995–1001. doi:10.1023/A:1008416911099. PMID: 9818074.

50. Yu J, Li S, Chen D, Liu D, Guo H, Yang C, Zhang W, Zhang L, Zhao G, Tu X. et al. IMM0306, a fusion protein of CD20 mAb with the CD47 binding domain of SIRPalpha, exerts excellent cancer killing efficacy by activating both macrophages and NK cells via blockade of CD47-SIRPalpha interaction and fcγR engagement by simultaneously binding to CD47 and CD20 of B cells. Leukemia. 2023;37:695–98. doi:10.1038/s41375-022-01805-9. PMID: 36575242.

51. Ryan AM, Sokolowski SA, Ng CK, Shirai N, Collinge M, Shen AC, Arrington J, Radi Z, Cummings TR, Ploch SA. et al. Comparative nonclinical assessments of the proposed biosimilar PF-05280586 and rituximab (MabThera(r)). Toxicol Pathol. 2014;42:1069–81. doi:10.1177/0192623313520351. PMID: 24604381.